Supplemental text, figures, and tables

"Movement between India and Eurasia since 60 Ma from new high resolution reconstructions of India-Somalia plate motion and rifting in eastern Africa"

by C. DeMets & S. Merkouriev

All of the figures and tables listed below are referenced in either the main document or this supplemental document. References for all of the papers that are cited herein are found in the main document.

Content list

1. *Supplemental Figure 1*: This regional-scale map identifies the locations of the other maps that are included amongst the thirteen supplemental figures.

2. *Supplemental Figure 2*: This map shows the along-track magnetic anomaly data used in the analysis and vertical derivative of the 1-minute gravity field (version 29 available at ftp://topex.ucsd.edu/pub/global_grav_1min; Sandwell et al. 2014). The map, which presents our data without any interpretations, is best viewed at several times magnification. The map area is identified in Supplemental Figure 1. Supplemental Figure 4 shows the same data with our interpretations and the magnetic lineations and fracture zone flow lines reconstructed with the rotations in Table 2 of the main document.

3. *Supplemental Figure 3*: Synthetic magnetic profile that identifies the Chron 6 to Chron 26 reversal correlation points that are used for our study.

4. *Supplemental Figure 4*: Along-track magnetic anomaly data from Supplemental Figure 2 with our interpretations and reconstructions of all 45 magnetic reversals and flow lines that are described in the main document. This graphic is best viewed when magnified 200 percent or more. See the figure caption for more relevant information.

5. *Supplemental Figure 5*: Reconstructions of all 45 magnetic reversals, fracture zone flow lines, and transform faults with Table 2 rotations overlaid on a 3-km-resolution bathymetric grid that we derived from depth measurements along the ship tracks that are displayed in Figure 2 of the main document. See Supplemental Figure 1 for the region covered by this map and this figure's caption for more relevant information.

6. *Supplemental Figure 6*: Carlsberg Ridge seafloor spreading rates from new best-fitting rotations calibrated to reversal ages from GTS12 (Ogg 2012), GTS20 (Ogg 2020), and MQSD20 (Malinverno *et al*. 2020).

7. *Supplemental Figure 7*: Southern Central Indian Ridge data reconstructions and seafloor spreading rate comparison.

8. *Supplemental Figure 8*: Comparison of finite opening poles from this study to those for previous studies.

9. *Supplemental Figure 9*: Timeline of the plate circuit rotations and interpolations that constrain the India-Eurasia rotations in Table 4 of the main document.

10. *Supplemental Figure 10*: Fits of Cande & Patriat (2015) Capricorn-Somalia rotations to magnetic lineations C23n.2o to C26no along the western Carlsberg Ridge (Panel A) and magnetic lineations C20n.1o to C23n.2o along the eastern Carlsberg Ridge (Panel B). See figure caption for further details. Supplemental Figure 1 shows the region that is covered by this map.

11. *Supplemental Figure 11*: Comparisons of Table 2 rotation fits to Cande & Patriat (2015) and Yakteesh et al. (2019) Somalia-Capricorn rotation fits for C20n.1o to C23n.2o. The Somalia-Capricorn rotations were adjusted for the post-16-Ma movement between the Capricorn and India plates for this comparison, as is indicated in the figure caption. Supplemental Figure 1 shows the region that is covered by this map.

12. *Supplemental Figure 12*: Fits of Yatheesh *et al*. (2019) Capricorn-Somalia rotations to magnetic lineations C23n.2o to C26no along the western Carlsberg Ridge (Panel A) and magnetic lineations C20n.1o to C23n.2o along the eastern Carlsberg Ridge (Panel B). See figure caption for further details. Supplemental Figure 1 shows the region that is covered by this map.

13. *Supplemental Figure 13*: Fits of Patriat & Segoufin (1988) Capricorn-Somalia rotations to magnetic lineations C23n.2o to C26no along the western Carlsberg Ridge (Panel A) and magnetic lineations C20n.1o to C23n.2o along the eastern Carlsberg Ridge (Panel B). See figure caption for further details. Supplemental Figure 1 shows the region that is covered by this map.

14. *Supplemental Table 1*: Somalia-India finite rotations with covariances tied to the India plate. The rotations in Table 2 of the main document have their covariances tied to the Somalia plate. Both sets of rotations were otherwise derived from the same data using the methodology described in the main document.

15. *Supplemental Table 2*: Somalia-India angular velocities with covariances tied to the India plate. These were derived from the rotations in Supplemental Table 1 and are appropriate for calculating plate velocities in a frame of reference that is tied to the India plate. Angular velocities that are appropriate for calculating plate velocities in a Somalia plate frame of reference are found in Table 3 of the main document.

16. *Supplemental Table 3*: Somalia-India finite rotations that best fit the same magnetic lineation data as were used to estimate the Table 2 rotations in the main document but that best fit the two Chain fracture zone flow lines at the western end of the Carlsberg Ridge instead of the Maldive and Rudra fracture zone flow lines that were used to estimate the Table 2 rotations. The rotation covariances are tied to the India plate, the same as for the rotations that are listed in Supplemental Table 1.

17. *Supplemental Table 4*: Capricorn-Somalia finite rotations compiled from sources listed in the table footnotes.

18. *Supplemental Table 5*: India-Eurasia angular velocities with covariances tied to the India plate. These were derived from the rotations in Table 4 of the main document and are appropriate for calculating plate velocities in an India plate frame of reference.

1 Tests of alternative flow line combinations

We evaluated three combinations of fracture zone flow lines to constrain our India-Somalia rotations at times older than Chron 20, as follows: (1) The Chain fracture zone at the western end of the Carlsberg Ridge, which consists of two sub-parallel strands (Fig. 5 in the main document). (2) The Maldive and Rudra fracture zones, which are located at the eastern end of the Carlsberg Ridge near the paleocenter of the India-Africa plate boundary at the time of Chron 20 (Fig. 5 in the main document). (3) All of the fracture zone flow lines.

Each of the above were combined with the 8984 magnetic reversal crossings, 14 fracture zone flow lines for C21 to the present, and four transform faults that are described in Section 2 of the main document and inverted in order to find their best least-squares misfits normalized by their associated degrees of freedom, *i.e.* ${\chi^2}_\nu$. The resulting values for ${\chi^2}_\nu$ for the three data sets in the order listed in the previous paragraph are 1.23, 1.41, and 2.44. Brief comparative discussions of these results follow.

The rotations that best fit the Chain fracture zone flow lines, which are given in Supplemental Table 3, have a misfit ${\chi^2}_\nu$ that is ≈15 percent better than for the rotations that best fit the Rudra and Maldive fracture zones (found in Table 2 of the main document). Nearly all the difference in the fit is attributable to smaller WRMS misfits for the two Chain fracture zone strands than for the Rudra and Maldive fracture zones for times between 55 and 45 Ma (compare the open and filled blue circles in Fig. 7 of the main document). The smaller misfits indicate that the magnetic reversal crossings for times older than C20 are more consistent with the Chain fracture zone constraints than for the Rudra and Maldive fracture zones.

The misfit for the rotations that simultaneously fit all the fracture zone flow lines is ∼50 percent higher for the fracture zone crossing misfit (χ^2 of 22,948 for 4787 degrees of freedom) than the sum of the squared fracture zone misfits for the separate inversions described above, for which χ^2 is only 15,714 for the same 4787 degrees of freedom. By implication, the rotation constraints from the two Chain fracture zone strands are inconsistent with those from the Rudra and Maldive fracture zones within their estimated uncertainties. The magnitude of the inconsistency is illustrated in Fig. 10a of the main document. The Chain fracture zone flow line that is predicted with our Table 2 rotations, which were derived from the Rudra and Maldive fracture zones, misfits the trace of the Chain fracture zone by ≈50 km or more along much of the flow line. In a similar manner, the rotations that were derived partly from the Chain fracture zone strands (Supplemental Table 3) predict a northern Maldive fracture zone flow line that disagrees with the observed trace by 25-50 km along much of the fracture zone (red line in Fig. 10b of the main document).

These flow line inconsistencies, which affect only our rotations for C20 and older times, may be caused by misinterpretations of the fracture zone locations as well as ambiguities in identifying the correct age(s) of the flow line seed points. These may constitute the most important limitation of our analysis. Previous authors have used a variety of flow lines and methodologies to constrain their pre-C20 India-Africa rotations (*e.g.* Cande *et al.* 2010; Eagles & Hoang 2014; Cande & Patriat 2015). In Section 5.2.2 of the main document, we show that their India-Somalia rotations misfit the flow lines we identified. Although these differences may be evidence for inaccuracies in some previous rotations, they may instead reflect differences in flow line selections, interpretations, and methodologies between previous studies and this study.

Although ${\chi^2}_\nu$ of 1.23 for the inversion with the Chain fracture zone strands for C26 to C20, is superior to that for the Rudra/Maldive fracture zones (${\chi^2}_\nu$ of 1.41), we adopt the Table 2 rotations, which best fit the Maldive and Rudra fracture zones, as our preferred estimates for three reasons. First, identifiable traces of both fracture zones exist north and south of the ridge, thereby reducing

the impact of any individual flow line misinterpretation on the overall solution. Second, the Rudra and Maldive fracture zones are located near the centroid of the Chron 20 paleo-spreading center. Errors in India-Somalia plate directions that are estimated along the central and southern portions of the paleo-spreading center will thus be smaller when estimated with the Table 3 angular velocities than with angular velocities that derive from a solution based on the Chain fracture zone flow lines at the western extreme of the plate boundary. Finally, the fits of the two solutions to the magnetic lineations, our most reliable data, differ insignificantly ($\chi^2{}_\nu$ of 1.00 versus 0.96). Adopting either set of flow lines thus results in only small changes in the estimated opening distances and hence seafloor spreading rates for times before Chron 20.

2 Southern Central Indian Ridge spreading rates

For part of our analysis, we estimated best-fitting rotations that reconstruct 15 magnetic reversals from the southern Central Indian Ridge, ranging from the old edge of C26 (59.2 Ma) to the young edge of C20 (49.2 Ma), and the trace of the southern Boussole fracture zone. These reversal crossings are described in Section 2.2 of the main document and displayed in Supplemental Figure 7. Fig. 17 of the main document shows the reversal crossings at their original locations. Before we inverted these data, we rotated the reversal crossings on the Capricorn plate (northeast of the Central Indian Ridge) to their equivalent India plate locations using the C5Cn.1 Capricorn-India finite rotation of Bull *et al*. (2010). Our inversions of the above data thus yield rotations that describe the movement of the India plate relative to the Somalia plate between 59.2 Ma and 49.2 Ma based solely on southern Central Indian Ridge data. Due to the short arc that is spanned by the data, the poles/rotations are poorly constrained and mostly useful for reconstructing the kinematic history of a limited region of the southern Central Indian Ridge during this period.

Supplemental Figures 7a and 7b show the magnetic lineations and flow lines reconstructed onto the Somalia plate with the best-fitting rotations from our inversion. The reversal WRMS misfits range from 1.6-4.1 km, comparable to those for our Carlsberg Ridge inversions (Fig. 7 in the main document). Supplemental Figure 7c compares the 60-40 Ma spreading rate histories along a C26-to-C20 flow line through the region that is shown in Supplemental Figure 7 as estimated with our new best fitting rotations (blue line), with the Table 3 India-Somalia angular velocities from our analysis of Carlsberg Ridge data, and with Capricorn-Somalia angular velocities that we estimated from finite rotations in Yahteesh *et al*. (2019) (dashed green line). After normalizing all the rates to GTS20, the India-Somalia spreading rates that are estimated with the newly derived best-fitting rotations (blue line in the figure) increase by ≈20 percent at 53 Ma, less than the ≈100 percent spreading rate pulse we estimated from the Carlsberg Ridge data during this period (Fig. 13a in the main document). The southern Central Indian Ridge spreading rates remain nearly steady from 53.2 Ma to 49.7 Ma and thus differ from the rate history indicated by our Table 3 angular velocities, which instead began to decline at 51.7 Ma (red lines in Supplemental Fig. 7c and Fig. 13a in the main document). The differences in how spreading rates evolved along the Carlsberg Ridge and southern Central Indian Ridge during this period may be due to their different locations with respect to the evolving stage pole location during this period or could instead indicate that the rotation noise is larger than is indicated by the formal rotation covariances. Further work is needed to discriminate between these possibilities.

3 Somalia plate absolute motion change: 31 to 18 Ma

We determined differential angular velocities that approximate the net changes in Antarctic-Somalia and Capricorn-Somalia relative motions from 31 Ma to 18 Ma as follows:

For the Antarctic-Somalia plate pair, we used the C17n.1y (36.6 Ma) and C12no (31.0 Ma) rotations and C5Ey (18.0 Ma) and C5n.1y (9.8) rotations from Table 9 of DeMets *et al*. (2021) to find stage angular velocities for the desired intervals before 31 Ma and after 19 Ma, *i.e*. we estimated $\dot{\omega}^{AN\rightarrow SM}_{17n.1y\rightarrow 12no}$ and $\dot{\omega}^{AN\rightarrow SM}_{5E\rightarrow 5n.1y}$. The Antarctic-Somalia differential angular velocity used for the calculations and figures in the main document is thus $\dot{\omega}_{17n.1y\rightarrow 12no}\ \dot{\omega}^{T}_{5E\rightarrow 5n.1y} = \Delta\dot{\omega}_{12no\rightarrow 5E}$.

For the Capricorn-Somalia plate pair, we used the C18n.2o (40.1 Ma) and C13no (33.7 Ma) rotations and C5Ey (18.1 Ma) and C5Bn.2 (15.2) rotations from Supplemental Table 4 to estimate stage angular velocities for the desired intervals before 31 Ma and after 19 Ma, *i.e*. we estimated $\dot{\omega}^{AN\rightarrow CP}_{18n.2o\rightarrow 13no}$ and $\dot{\omega}^{AN\rightarrow CP}_{5E\rightarrow 5Bn.2}$. The Capricorn-Somalia differential angular velocity used for the calculations and figures in the main document is thus $\dot{\omega}_{18n.2o\rightarrow 13no}\ \dot{\omega}^{T}_{5E\rightarrow 5Bn.2} = \Delta\dot{\omega}_{13no\rightarrow 5E}$.

Since the differential angular velocities indicated above are all small angle rotations, they are summed and differenced as vectors to high approximation, *i.e*.

$$\Delta\dot{\omega}^{IN\rightarrow SM}_{13ny\rightarrow 6ny} = (19.2°S, 96.0°E, 0.318°Myr^{-1}) = \Delta\dot{\omega}^{IN\rightarrow ABS}_{13ny\rightarrow 6ny} - \Delta\dot{\omega}^{SM\rightarrow ABS}_{13ny\rightarrow 6ny} \quad (1)$$

$$\Delta\dot{\omega}^{AN\rightarrow SM}_{12no\rightarrow 5E} = (26.0°S, 138.7°E, 0.149°Myr^{-1}) = \Delta\dot{\omega}^{AN\rightarrow ABS}_{12no\rightarrow 5E} - \Delta\dot{\omega}^{SM\rightarrow ABS}_{12no\rightarrow 5E} \quad (2)$$

$$\Delta\dot{\omega}^{CP\rightarrow SM}_{13no\rightarrow 5E} = (8.6°S, 199.0°E, 0.197°Myr^{-1}) = \Delta\dot{\omega}^{CP\rightarrow ABS}_{13no\rightarrow 5E} - \Delta\dot{\omega}^{SM\rightarrow ABS}_{13no\rightarrow 5E} \quad (3)$$

The three differential angular velocities, which are located in Fig. 20a of the main document and were used to predict the 31-18 Ma net velocity changes at Somalia plate locations depicted in Fig. 20b of the main document, describe the net velocity changes of the three plate pairs for slightly different intervals, namely 33.21-18.64 Ma (India-Somalia), 30.98-18.00 Ma (Antarctic-Somalia), and 33.73-18.00 Ma (Capricorn-Somalia) assuming reversal ages from the GTS20 time scale. They nonetheless approximate the net velocity changes across the Somalia plate seafloor spreading centers from 31 Ma to 18 Ma, the interval of interest.

Equations (1)-(3) in the main document are underdetermined with respect to solving for the final term in the above equations, namely the angular velocity of change for the Somalia plate relative to the mantle for 31-18 Ma. Nonetheless, the similarities in the three differential angular velocities that are estimated in Equations 1-3 constitute qualitative evidence for a common source for the observed changes, namely a change in the Somalia plate's absolute motion. Absent any additional constraints that allow us to solve uniquely for $\Delta\dot{\omega}^{SM\rightarrow ABS}_{31\rightarrow 18}$, we averaged the three differential angular velocities to find a best estimate for their common component. Doing so gives $\Delta\dot{\omega}^{SM\rightarrow ABS}_{31\rightarrow 18} = (23.9°S, 134.5°W, 0.164°Myr^{-1})$.

Using the same methods as are described above, we estimated a 33-20 Ma differential angular velocity for the Somalia plate relative to the mantle from the C18n.2o (40.1 Ma), C13ny (33.2 Ma), C6no (19.5 Ma), and C5Cn.1 (16.0 Ma) rotations in Table S2 of Maher *et al*. (2015). For this case, we find $\Delta\dot{\omega}^{SM\rightarrow ABS}_{13no\rightarrow 6ny} = (40.4°S, 10.1°W, 0.164°Myr^{-1})$.

4 India-Somalia pole comparison

India-Somalia finite poles for C1n back to C6 agree closely with those estimated by DeMets *et al*. (2020) (Fig. 11b in the main document), as might be expected given that they were derived from many of the same data and use the same fitting methodology. Finite poles for C1n to C6 estimated by Merkouriev & DeMets (2006), which use many of the same reversal crossings but different fracture zone data and a different fracture zone fitting methodology, also agree closely with our new estimates (not shown in Fig. 11b).

We compared our newly estimated finite rotation poles for C13-C26 to poles estimated in five previous studies (Supplemental Figure 8). India-Somalia poles for C26 to C21 from Royer *et al*. (2002) were estimated from Carlsberg Ridge reversal crossings and flow lines (Supplemental Figure 8a). Poles from Eagles & Hoang (2014) were also estimated from Carlsberg Ridge reversal crossings and flow lines from the Carlsberg and Central Indian Ridges (Supplemental Figure 8a). India-Somalia poles from Seton *et al*. (2012) are also included although the data that were used to estimate those poles are not specified in that study.

Poles from studies that estimate India-Somalia plate motion without any constraints from Carlsberg Ridge data are depicted in Supplemental Figure 8b after correcting each pole for the movement of the Capricorn plate relative to India since 16 Ma (*i.e*. $\hat{A}^{CP\rightarrow IN}_{5Cn.1\rightarrow 0}\hat{A}^{SM\rightarrow CP}$ from Section 4.3.4). These include C20-and-older Capricorn-Somalia rotations that were derived by summing Africa-Antarctic and Antarctic-Capricorn rotations that best reconstruct data from the Southwest Indian and Southeast Indian ridges (Cande & Patriat 2015), and C20-and-older Capricorn-Somalia rotations estimated from Central Indian Ridge data south of 10°S (Yatheesh *et al*. 2019).

The poles in the former group generally agree well except for those of Seton *et al*. (2012), which are consistently 4-5 degrees farther north than the other poles (Supplemental Figure 8a). The Royer *et al*. (2002), Eagles & Hoang (2014), and our poles all migrate eastward from Chron 26 to Chron 23, after which the former poles continue migrating eastward and our poles migrate northward. We suspect that these differences are caused by the different fracture zone constraints that were used in the various studies. The Capricorn-Somalia poles corrected for India-Capricorn movement also migrate eastward from C26 to C23 but migrate gradually northward after C23 (Supplemental Figure 8b), similar to our own. The similar pole paths are perhaps surprising given that the three pole sequences displayed in Supplemental Figure 8b were estimated independently from Carlsberg Ridge data, southern Central Indian Ridge data, and data from the Southwest Indian and Southeast Indian ridges.

5 Carlsberg Ridge Chron 20 and older fits and misfits: Previous studies

As part of our analysis, we examined the fits of previous Capricorn-Somalia rotation estimates to the Carlsberg Ridge and northern Central Indian Ridge magnetic lineations, with a goal of evaluating whether errors in our India-Somalia and/or previous Capricorn-Somalia rotations might be the reason for the large misfits to Chrons 23 and 24 that are described in Section 5.4 of the main document. We used three sequences of Capricorn-Somalia plate rotations for the analysis. Cande & Patriat (2015) estimated Capricorn-Somalia for Chron 20 and older times by combining Africa-Antarctic and Antarctic-Capricorn rotations based on their reconstructions of Southwest India and Southeast Indian ridge data. Their rotations thus do not use any data from the southern Central Indian Ridge in order to estimate Capricorn-Somalia rotations. In contrast, Patriat & Segoufin

(1988) and Yatheesh *et al*. (2019) both estimated Capricorn-Somalia rotations for Chron 20 and older times by reconstructing magnetic lineations across the southern Central Indian Ridge. These three independent rotation sequences were estimated with different methodologies, different data, and in one case by enforcing closure of the Somalia-Capricorn-Antarctic plate circuit. They consequently sample different kinds of rotation errors and are thus useful for our effort to evaluate the role of rotation errors in the aforementioned C23 and C24 misfits.

Supplemental Figure 10 shows C20 and older magnetic lineations along the Carlsberg Ridge reconstructed onto the India plate after correcting the Cande & Patriat (2015) Capricorn-Somalia rotation sequence to an India plate frame of reference with the Bull *et al*. (2010) C5Cn.1 India-Capricorn rotation (*i.e*. $\hat{A}^{CP\rightarrow IN}_{5Cn.1\rightarrow 0}\hat{A}^{SM\rightarrow CP}$). Along the eastern Carlsberg Ridge (Supplemental Figure 10b) the Somalia-side magnetic lineations reconstructed with Cande & Patriat's closure-predicted rotations underrotate their India-side counterparts for C20n.1o and C21n.1 by only 15-25 km, close to the likely uncertainties. Crossings of C22n.1o are overrotated a similar amount but are misaligned more than 50 km with respect to their expected flow line. Crossings of C23n.2o are underrotated by $\sim$30 km. In contrast to these misfits, the same closure-predicted rotations closely realign C20n.1o, C21n.1o, and C23n.2o on the Somalia plate east of the Rudra/Maldive fracture zones (Supplemental Figure 11a).

Along the western Carlsberg Ridge, where C23n.2o through C26 are well mapped, reconstructions with the Cande & Patriat (2015) rotations, also corrected for Capricorn-India motion, yield an excellent closure-predicted fit for C23n.2o (Supplemental Figure 10a), but underrotate the C24, C25, and C26 magnetic lineations by 50-90 km. The Cande & Patriat's (2015) closure-enforced Capricorn-Somalia rotations thus reconstruct India-Somalia magnetic lineations along the eastern Carlsberg Ridge except for C22 to within a few tens of kms back to C23n.2o if they are corrected for post-16 Ma Capricorn-India plate movement.

In contrast to the successful realignments of eastern Carlsberg Ridge magnetic lineations back to C23n.2o with the Cande & Patriat (2015) rotations, similarly corrected best-fitting rotations from Yatheesh *et al*. (2019) and Patriat & Segoufin (1988), both derived via reconstructions of data from the southern Central Indian Ridge, fit the eastern Carlsberg Ridge data more poorly (Supplemental Figures 12 and 13). The systematic misfits for both sets of rotations are frequently larger than 50 km and occasionally more than 200 km. The misfits mostly consist of underrotations, although the corrected Patriat & Segoufin (1988) rotation for C22n.1o overrotates the conjugate lineations by more than 200 km along the eastern Carlsberg Ridge (Supplemental Figure 13b).

We interpret the smaller misfits for Cande & Patriat's (2015) closure-predicted rotations as evidence that circuit closure constraints that are imposed on Capricorn-Somalia rotations by data from the Southwest Indian and Southeast Indian ridges improve the accuracy of the Capricorn-Somalia rotations back to at least C23n.2o.

Although errors in the C24 to C26 rotations from all three sources listed above might explain their large misfits for the C24 through C26 magnetic lineations, the misfits may also be evidence that either the Somalia or India plate deformed before the time of Chron 23 (51 Ma). As is described in the main document, we were unable to identify a single set of Somalia-IndoCapricorn rotations that satisfactorily fit the C23n.2o, C24n.1n, C24n.3n, or C24n.3o magnetic lineations from the Carlsberg and Central Indian Ridges. The poor fits might be caused by a misidentification of the C24 magnetic anomaly sequence or inconsistency in one or more of the fracture zone flow lines that are included in our inversions (Section 5.4 of the main document). Alternatively, deformation within the Somalia and/or IndoCapricorn plate earlier than the C23n.2o/C24n.1n ($\approx$52 Ma) may also explain the poor fits.

The Cande & Patriat (2015) closure-derived rotations underrotate the C25 and C26 magnetic

lineations by 50 km and 90 km, respectively, along the western Carlsberg Ridge (Supplemental Figure 10a). In contrast, our Table 2 C25 and C26 rotations realign the C25 and C26 lineations more successfully along the southern Central Indian Ridge (Fig. 26 in the main document). The latter suggests that future efforts to unify the Chron 25 and 26 data from the entire IndoCapricorn-Africa paleospreading center may be successful.

Overall, our results suggest that the Carlsberg Ridge and Central Indian Ridge magnetic lineations back to Chron 22 and possibly as old as C23n.1n may have been created along the same paleospreading boundary. The much larger misfits of all the rotations for the C23n.2o and C24 magnetic lineations but relatively smaller misfits for the C25 and C26 magnetic lineations are hard to explain. An effort to reconcile all the post-Chron C27 magnetic lineation and fracture zone data between the Owen fracture zone and Rodriguez Triple Junction, including a suitable correction for India-Capricorn plate motion during the past 16 Myr, is clearly warranted, but beyond the scope of this work.

Table 1: (Supplemental) Somalia-India finite rotations

Chron	Lat.	Long.	Ω	Rotation covariances*					
	(°N)	(°E)	(degrees)	a	b	c	d	e	f
1n	23.39	32.50	-0.318	6.6	12.8	1.1	25.5	2.1	0.3
2n	23.91	34.01	-0.730	6.3	12.5	1.0	25.6	2.2	0.5
2An.1	23.37	33.35	-1.064	6.4	12.4	1.0	25.2	2.1	0.4
2An.3	21.33	37.06	-1.631	7.0	13.9	1.1	28.6	2.4	0.5
3n.1	23.63	31.27	-1.693	6.6	13.1	1.1	26.9	2.2	0.4
3n.4	22.69	34.14	-2.231	7.2	14.3	1.0	29.6	2.4	0.7
3An.1	23.72	31.15	-2.399	12.6	24.5	1.0	50.9	3.6	1.5
3An.2	23.05	32.94	-2.757	10.6	21.0	0.8	44.7	3.3	1.6
4n.1	23.27	32.36	-3.024	14.1	28.8	1.4	62.2	4.7	1.8
4n.2	22.85	32.44	-3.312	11.4	23.4	1.2	50.9	3.7	1.2
4A	23.70	30.97	-3.607	10.0	19.9	1.5	43.1	4.8	1.7
5n.1	23.12	31.42	-3.928	11.4	22.8	2.0	48.0	5.1	1.3
5n.2	23.51	31.55	-4.438	9.4	19.0	2.2	40.5	5.2	1.3
5An.2	24.13	29.73	-4.858	11.9	23.7	2.2	49.7	5.3	1.3
5AC	23.05	32.27	-5.653	15.8	33.0	3.3	71.9	8.0	1.7
5AD	24.39	29.96	-5.800	12.7	27.3	2.8	61.5	6.9	1.5
5Cn.1	24.74	29.83	-6.410	12.6	28.1	3.0	65.5	7.8	1.7
5D	24.52	30.87	-7.195	11.7	24.7	2.2	56.3	6.6	1.9
5E	24.98	30.59	-7.611	16.2	35.3	3.6	82.9	10.8	3.1
6ny	24.91	31.19	-8.091	25.4	55.7	7.0	129.7	18.4	4.4
6no	25.41	30.47	-8.405	20.5	45.3	6.1	106.0	15.2	3.4
6AAr.2n	26.61	29.29	-8.971	7.8	16.3	2.6	37.4	7.4	2.7
8n.1n	27.54	30.30	-9.992	20.9	47.4	9.5	111.2	23.9	6.8
11n.1n	24.20	37.13	-13.122	34.3	77.1	14.8	177.3	36.1	9.7
13ny	24.31	39.55	-14.828	21.4	47.8	9.8	107.9	21.3	4.9
18n.1n	22.74	42.86	-17.970	114.8	258.9	36.6	585.9	81.8	12.0
18n.2o	22.82	43.08	-18.608	20.0	45.1	6.2	102.8	13.6	2.1
19ny	23.05	42.72	-18.918	91.9	213.4	16.2	497.8	37.2	3.0
20n.1n	23.40	42.34	-19.221	11.0	24.9	2.7	58.0	5.6	0.8
20n.1o	22.72	42.71	-20.126	9.8	20.3	1.6	43.9	3.1	0.3
21n.1n	21.97	42.42	-21.365	7.7	15.6	1.0	33.8	1.9	0.2
21n.1o	21.96	40.93	-21.919	16.7	39.4	6.5	97.0	16.1	3.3
22n.1n	19.88	41.63	-24.571	22.6	51.8	8.0	122.8	19.3	4.3
22n.1o	19.35	41.39	-25.678	14.9	32.3	6.5	75.5	15.4	3.8
23n.1n	19.67	39.35	-26.352	17.3	37.4	9.5	83.3	21.7	8.2
23n.2y	19.25	39.52	-27.186	21.2	43.6	10.5	97.0	23.9	7.3
23n.2o	19.19	38.31	-27.835	21.3	45.7	14.4	104.0	33.6	12.5
24n.1n	17.57	38.99	-31.503	930.8	1723.0	639.8	3192.8	1186.2	447.9
24n.1r	17.78	38.54	-31.855	998.8	1955.7	744.8	3495.5	1351.1	534.8
24n.3n	18.67	36.90	-30.509	455.7	849.2	313.4	1585.6	585.4	223.4
24n.3o	18.45	36.34	-30.980	485.7	949.3	355.1	1859.1	696.5	262.4
25y	21.99	26.32	-28.021	115.8	231.8	117.9	466.2	237.5	123.2

25o	21.58	26.36	-28.840	155.7	304.7	156.5	598.6	307.8	159.3
26y	20.94	25.92	-30.750	216.2	418.3	239.1	811.4	464.2	268.5
26o	20.63	26.11	-31.444	445.1	868.9	500.5	1698.7	979.1	566.4

These finite rotations, which reconstruct the India plate onto the Somalia plate, were estimated from the same data as were the rotations from Table 2 of the main document, but have covariances that were calculated in a frame of reference tied to the India plate. The covariances thus describe uncertainties in the locations of points that are rotated from the India plate onto Somalia. The rotation angles Ω are positive CCW. The Cartesian covariances have units of 10^{-8} radians^2. Further information is found in the Table 2 footnotes.

Table 2: (Supplemental) Somalia-India stage angular velocities

Interval	Lat.	Long.	$\dot{\omega}$	Covariances					
	(°N)	(°E)	($^\circ$ Myr^{-1})	a	b	c	d	e	f
1n-0	23.39	32.50	-0.412	0.11	0.21	0.02	0.43	0.04	0.00
2n-1n	24.32	35.19	-0.411	0.13	0.25	0.02	0.51	0.04	0.01
2An.1-2n	22.16	31.92	-0.407	0.19	0.37	0.03	0.76	0.07	0.01
2An.3-2An.1	17.44	43.76	-0.574	0.13	0.26	0.02	0.54	0.05	0.01
3n.1-2An.3	27.58	-43.91	-0.305	0.38	0.77	0.07	1.59	0.15	0.03
3n.4-3n.1	19.61	42.89	-0.521	0.12	0.25	0.02	0.52	0.05	0.01
3An.1-3n.4	29.79	-6.24	-0.261	0.31	0.62	0.04	1.30	0.11	0.04
3An.2-3An.1	18.46	44.45	-0.522	0.45	0.90	0.05	1.94	0.17	0.07
4n.1-3An.2	25.26	26.19	-0.331	0.37	0.75	0.04	1.64	0.14	0.06
4n.2-4n.1	18.52	33.34	-0.492	0.70	1.48	0.10	3.29	0.30	0.10
4A-4n.2	31.35	13.50	-0.316	0.21	0.44	0.04	0.99	0.11	0.03
5n.1-4A	16.65	36.37	-0.476	0.44	0.90	0.09	1.98	0.25	0.08
5n.2-5n.1	26.60	32.47	-0.402	0.12	0.25	0.03	0.55	0.08	0.02
5An.2-5n.2	28.26	10.13	-0.313	0.10	0.21	0.03	0.45	0.06	0.02
5AC-5An.2	16.57	46.90	-0.655	0.16	0.35	0.04	0.76	0.10	0.02
5AD-5AC	36.37	-37.40	-0.334	0.35	0.77	0.10	1.78	0.25	0.06
5Cn.1-5AD	28.05	28.35	-0.448	0.12	0.29	0.04	0.69	0.10	0.02
5D-5Cn.1	22.94	39.29	-0.629	0.14	0.32	0.04	0.77	0.12	0.03
5E-5D	32.47	24.83	-0.546	0.43	0.97	0.12	2.35	0.37	0.11
6ny-5E	24.02	40.57	-0.771	0.97	2.21	0.32	5.40	0.91	0.25
6no-6ny	35.13	9.82	-0.374	0.50	1.17	0.20	2.93	0.55	0.15
6AAr.2n-6no	40.46	8.18	-0.285	0.05	0.12	0.02	0.31	0.07	0.02
8n.1n-6AAr.2n	35.98	38.99	-0.306	0.02	0.05	0.01	0.13	0.03	0.01
11n.1n-8n.1n	14.76	56.80	-0.839	0.03	0.07	0.02	0.17	0.04	0.01
13ny-11n.1n	26.02	57.56	-0.444	0.03	0.07	0.02	0.17	0.05	0.02
18n.1n-13ny	16.97	58.25	-0.634	0.05	0.11	0.02	0.26	0.04	0.01
18n.2o-18n.1n	25.74	48.66	-0.383	0.34	0.91	0.23	2.47	0.63	0.17
19ny-18n.2o	30.82	18.88	-0.350	1.15	2.73	0.29	6.57	0.72	0.12
20n.1n-19ny	37.27	13.56	-0.296	0.47	1.39	0.29	4.21	0.89	0.20
20n.1o-20n.1n	9.83	51.98	-0.750	0.11	0.25	0.04	0.66	0.11	0.03
21n.1n-20n.1o	9.53	40.56	-0.457	0.02	0.04	0.01	0.10	0.02	0.00
21n.1o-21n.1n	8.51	-1.03	-0.498	0.09	0.22	0.04	0.57	0.10	0.02
22n.1n-21n.1o	4.70	50.08	-2.499	0.27	0.67	0.16	1.72	0.43	0.14
22n.1o-22n.1n	7.11	39.21	-1.440	0.49	1.19	0.36	3.09	0.95	0.34
23n.1n-22n.1o	9.03	-12.93	-1.005	0.23	0.53	0.17	1.26	0.43	0.19
23n.2y-23n.1n	7.56	47.21	-3.072	4.48	9.55	3.43	21.77	7.70	3.65
23n.2o-23n.2y	4.60	0.93	-1.248	0.83	1.79	0.71	4.13	1.67	0.79
24n.1n-23n.2o	7.22	46.77	-4.625	14.28	26.48	9.99	49.18	18.60	7.26
24n.3n-24n.1n	-1.55	-93.20	-2.209	26.51	46.51	26.11	81.95	45.35	27.16
24n.3o-24n.3n	-2.37	11.41	-0.858	21.74	39.81	20.27	73.53	36.53	20.03
25y-24n.3o	-5.08	-88.76	-1.842	0.47	0.93	0.65	1.84	1.29	0.92
25o-25y	8.71	30.78	-1.519	8.33	15.59	10.68	29.41	19.73	14.81

26y-25o	10.25	22.67	-1.496	2.10	3.81	2.80	6.98	5.01	3.94
26o-26y	9.62	36.83	-2.586	84.77	152.96	111.22	280.58	195.98	153.02

These angular velocities specify Somalia relative to India plate motion for the listed magnetic reversal interval. The angular rotation rates $\dot{\omega}$, which are positive anticlockwise, are normalized to the GTS20 magnetic reversal ages in Supplemental Table 1. The angular velocities and Cartesian covariances, which are tied to the India plate, are derived from the Supplemental Table 1 finite rotations, which have covariances that are also tied to the India plate. The covariances, which have units of 10^{-6} radians^2 Myr^{-2}, The footnotes to Table 2 in the main document give further information about the covariances.

Table 3: (Supplemental) India-Somalia finite rotations

Chron	Lat.	Long.	Ω	Rotation covariances*					
	(°N)	(°E)	(degrees)	a	b	c	d	e	f
1n	25.39	29.26	0.297	6.6	12.8	1.1	25.5	2.0	0.3
2n	24.50	33.21	0.714	6.8	13.4	1.0	27.4	2.1	0.4
2An.1	24.15	32.05	1.027	6.5	12.5	0.9	24.9	1.9	0.3
2An.3	21.79	36.45	1.595	7.0	13.6	0.9	27.1	2.0	0.4
3n.1	23.90	30.86	1.677	6.7	12.9	0.9	25.6	1.8	0.3
3n.4	23.06	33.66	2.197	7.6	14.6	0.7	29.5	1.8	0.6
3An.1	23.79	30.83	2.384	13.2	24.5	0.4	49.0	2.4	1.4
3An.2	23.42	32.42	2.717	11.2	21.3	0.3	43.8	2.3	1.4
4n.1	23.57	31.94	2.992	15.5	30.1	0.6	62.0	3.0	1.5
4n.2	23.08	32.10	3.283	12.3	24.1	0.5	49.9	2.1	1.0
4A	23.58	31.22	3.628	11.1	20.8	0.8	42.7	3.4	1.5
5n.1	23.34	30.95	3.884	12.6	23.8	1.3	47.4	3.3	0.9
5n.2	23.53	31.61	4.442	10.5	19.9	1.4	39.9	3.5	0.9
5An.2	24.09	29.86	4.869	12.3	22.7	0.9	44.5	2.6	0.9
5AC	23.11	32.20	5.640	17.6	33.7	1.6	67.4	4.0	1.0
5AD	24.52	29.70	5.767	14.8	29.2	1.4	60.0	3.3	0.8
5Cn.1	24.83	29.64	6.382	15.0	30.0	1.3	63.0	3.6	0.9
5D	24.60	30.77	7.176	10.8	19.8	-0.1	40.5	1.3	1.1
5E	25.02	30.44	7.589	20.6	39.5	1.1	82.2	4.6	1.8
6ny	25.31	30.50	7.956	30.0	58.1	3.1	119.6	8.3	2.2
6no	25.46	30.28	8.375	26.1	50.2	2.5	102.0	6.1	1.4
6AAr.2n	26.71	29.06	8.927	13.8	26.3	1.9	53.8	5.4	1.6
8n.1n	27.66	30.13	9.951	27.4	52.9	5.7	105.9	13.1	3.1
11n.1n	24.39	36.87	13.020	49.1	94.1	11.6	183.9	23.2	2.8
13ny	23.92	39.29	14.758	29.0	51.7	3.7	92.5	6.3	0.9
18n.1n	22.38	42.69	17.950	191.0	335.5	9.7	590.4	16.6	1.8
18n.2o	22.47	42.91	18.583	47.3	83.5	0.0	148.3	-0.1	0.8
19ny	22.76	42.49	18.821	121.0	206.1	-10.2	352.1	-17.5	1.4
20n.1n	23.04	42.28	19.181	45.0	76.6	-1.0	131.0	-1.8	0.6
20n.1o	22.59	42.37	19.913	23.9	37.9	-1.8	61.3	-3.2	0.5
21n.1n	21.83	42.16	21.184	13.5	20.7	-1.0	32.7	-1.7	0.3
21n.1o	21.99	40.58	21.678	301.3	571.6	19.3	1087.9	37.7	2.9
22n.1n	20.56	41.83	24.670	56.8	100.1	4.0	179.7	7.9	1.9
22n.1o	20.36	41.30	25.461	105.1	189.8	8.2	347.1	14.8	1.5
23n.1n	20.30	39.61	26.467	30.6	49.4	2.0	84.4	6.2	3.4
23n.2y	20.12	39.51	27.052	73.2	119.6	6.2	199.0	10.6	1.7
23n.2o	20.04	38.54	27.921	49.4	80.8	3.1	135.8	5.3	1.2
24n.1n	19.07	39.02	31.309	1655.0	2402.8	172.1	3493.3	251.2	20.3
24n.1r	18.93	38.84	32.034	1007.6	1464.8	98.4	2132.9	144.0	11.4
24n.3n	19.59	37.00	30.522	859.7	1255.8	75.0	1837.9	110.7	8.6
24n.3o	19.50	36.52	31.021	299.6	443.8	15.8	659.0	23.3	1.1
25y	21.66	26.20	27.945	322.7	472.3	9.1	693.1	14.0	1.6

25o	21.21	26.29	28.797	185.2	265.9	7.6	383.4	11.2	0.8
26y	20.91	25.74	30.625	685.4	987.0	4.9	1424.2	8.7	2.6
26o	20.68	26.17	31.475	1384.7	1984.9	-0.1	2847.5	0.0	0.9

These finite rotations, which reconstruct the Somalia plate onto the India plate, best fit nearly all the same data as do the rotations from Table 2 of the main document but substitute the Chain fracture zone flow lines described in the main document for the Maldive and Rudra fracture zone flow lines to constrain the plate motion before Chron 20 time. The covariances were calculated in a frame of reference tied to the India plate and thus describe uncertainties in the locations of points that are rotated from the India plate onto Somalia. The rotation angles Ω are positive CCW. The Cartesian covariances have units of 10^{-8} radians^2. Further information is found in the Table 2 footnotes.

Table 4: (Supplemental) Capricorn-Somalia finite rotations

Chron	Age	Lat.	Long.	Ω	Rotation covariances*					
	Ma	(°N)	(°E)	(degrees)	a	b	c	d	e	f
1n	0.773	10.24	52.04	-0.527	10.3	12.0	-8.7	22.2	-11.1	7.6
2n	1.775	10.28	49.54	-1.170	23.4	19.7	-17.6	31.5	-16.5	13.9
2An.1	2.595	10.84	48.97	-1.675	12.8	15.9	-9.7	28.5	-12.8	7.9
2An.3	3.596	13.39	49.81	-2.228	19.4	17.3	-15.5	30.2	-14.0	12.8
3n.4	5.235	10.27	49.16	-3.390	28.0	34.2	-22.2	62.7	-27.5	18.7
3An.1	6.023	12.45	48.94	-3.676	49.3	59.7	-39.3	94.6	-49.1	32.5
3An.2	6.727	11.81	49.21	-4.193	81.6	96.5	-67.2	130.9	-80.5	56.3
4n.2	8.125	11.48	49.82	-5.104	38.3	37.0	-34.7	51.9	-33.8	32.1
4A	9.105	13.81	48.29	-5.279	64.1	87.9	-50.3	154.5	-70.8	41.1
5n.1	9.786	12.21	47.78	-5.767	176.5	291.2	-120.3	536.9	-196.8	84.4
5n.2	11.056	13.88	46.91	-6.247	75.2	95.4	-56.5	209.8	-72.7	44.7
5An.2	12.474	14.13	45.87	-6.967	56.4	79.6	-40.8	217.5	-55.6	32.2
5AD	14.609	15.98	44.53	-7.823	132.5	272.3	-91.3	646.9	-182.9	68.1
5Bn.2	15.160	16.65	44.04	-7.995	177.2	355.3	-127.7	860.7	-245.0	100.3
5Cn.1	15.974	15.06	44.97	-8.915	58.9	101.0	-42.5	225.7	-69.4	33.6
5Cn.3	16.721	15.59	44.53	-9.320	37.1	72.1	-25.4	178.4	-47.6	19.5
5D	17.235	16.17	43.97	-9.528	64.0	140.7	-39.9	350.2	-84.9	27.9
5E	18.007	16.01	44.37	-10.178	70.2	134.8	-46.3	315.9	-85.6	33.5
6ny	18.636	17.31	43.37	-10.297	143.0	243.6	-97.0	531.5	-161.1	70.3
6no	19.535	17.23	43.29	-10.883	51.5	109.9	-34.7	293.7	-71.0	25.6
8n.2o	25.987	14.80	46.00	-15.400	-	-	-	-	-	
13no	33.726	16.32	47.69	-18.930	150.8	451.5	-146.8	1489.5	-474.1	163.1
18n.2o	40.073	16.76	48.42	-22.220	334.1	1143.2	-324.9	4122.9	-1157.8	340.0
20n.1n	42.196	17.13	47.92	-23.180	638.1	2243.2	-654.7	8019.2	-2343.1	699.7
20n.1o	43.450	17.91	47.20	-23.400	205.0	720.0	-212.3	2636.3	-756.1	244.0
21n.1n	46.235	17.93	46.16	-24.220	1248.8	4546.5	-1267.1	16782.0	-4657.6	1323.9
21n.1o	47.760	15.97	46.60	-26.390	255.3	948.0	-250.5	3555.4	-934.1	255.3
22n.1o	49.666	18.47	42.43	-26.150	275.3	1014.5	-249.7	3800.3	-932.3	242.0
23n.2o	51.724	15.98	41.29	-29.370	303.1	1091.3	-251.1	3994.7	-916.0	231.5
24n.3o	53.900	15.77	38.83	-31.310	471.3	1710.5	-361.7	6294.3	-1323.9	300.6

These rotations reconstruct the Capricorn plate onto the Somalia plate. The rotation angles Ω are positive CCW. The covariances describe uncertainties in points that are rotated from the Capricorn plate onto Somalia. The 3x3 Cartesian covariances, which have units of 10^{-8} radians^2, can be reconstructed using information from Table 2 of the main document. The sources of the rotations are as follows: C1-C6no - Supplemental Table 3 of Bull *et al*. (2010) and covariances from Supplemental Table 1 of the same paper. C8n.2o - Patriat & Segoufin (1988). No covariances are available for this rotation. C13-C24 - Table 2 of Cande *et al*. (2010). The covariances in Columns "c" and "d" of Table 2 of Cande *et al*. (2010) were misplaced and should instead be in Columns "d" and "c". The error is corrected in this table. The Cande *et al*. covariances listed above are divided by the $\hat{\kappa}$ values in Table 2 of Cande *et al*.

Table 5: (Supplemental) India-Eurasia stage angular velocities

Interval	Lat.	Long.	$\dot{\omega}$	Covariances					
	(°N)	(°E)	(° Myr^{-1})	a	b	c	d	e	f
1n-0	-27.24	202.25	-0.487	0.17	-0.05	0.12	0.18	-0.11	0.16
2n-1n	-30.00	204.54	-0.481	0.22	-0.07	0.15	0.22	-0.15	0.20
2An.1-2n	-29.67	201.71	-0.478	0.39	-0.12	0.25	0.36	-0.25	0.34
2An.3-2An.1	-24.41	215.99	-0.623	0.31	-0.10	0.19	0.28	-0.20	0.27
3n.1-2An.3	-31.87	138.85	-0.399	1.04	-0.34	0.59	0.90	-0.69	0.92
3n.4-3n.1	-23.37	216.11	-0.568	0.37	-0.13	0.21	0.32	-0.26	0.34
3An.1-3n.4	-30.32	170.45	-0.337	0.75	-0.23	0.42	0.71	-0.53	0.71
3An.2-3An.1	-20.85	217.81	-0.561	1.05	-0.32	0.58	1.03	-0.75	1.01
4n.1-3An.2	-27.25	196.55	-0.390	0.86	-0.25	0.47	0.84	-0.60	0.81
4n.2-4n.1	-20.98	205.11	-0.542	1.69	-0.48	0.93	1.63	-1.12	1.54
4A-4n.2	-31.33	183.40	-0.386	0.62	-0.17	0.34	0.54	-0.38	0.55
5n.1-4A	-19.00	208.38	-0.512	1.36	-0.31	0.71	1.09	-0.76	1.17
5n.2-5n.1	-28.81	202.90	-0.445	0.44	-0.08	0.22	0.32	-0.23	0.38
5An.2-5n.2	-30.83	181.61	-0.380	0.42	-0.05	0.19	0.29	-0.21	0.37
5AC-5An.2	-22.10	220.83	-0.695	0.66	-0.04	0.28	0.45	-0.32	0.56
5AD-5AC	-38.03	144.70	-0.453	1.68	-0.08	0.70	1.05	-0.71	1.26
5Cn.1-5AD	-31.76	196.99	-0.540	0.77	-0.04	0.30	0.40	-0.27	0.48
5D-5Cn.1	-26.19	209.50	-0.703	0.99	-0.10	0.35	0.47	-0.33	0.53
5E-5D	-30.08	193.49	-0.661	2.92	-0.36	0.88	1.42	-1.00	1.46
6ny-5E	-19.74	210.73	-0.882	4.90	-0.54	1.42	2.74	-1.67	2.43
6no-6ny	-13.37	184.50	-0.574	2.69	-0.41	0.82	1.61	-1.02	1.42
6AAr.2n-6no	-46.32	198.57	-0.352	0.81	-0.16	0.05	0.36	-0.11	0.14
8n.1n-6AAr.2n	-38.70	179.48	-0.597	0.37	-0.03	-0.03	0.15	-0.01	0.02
11n.1n-8n.1n	-22.65	219.43	-0.934	0.16	0.02	0.00	0.08	-0.02	0.04
13ny-11n.1n	-38.87	201.71	-0.636	0.22	0.03	-0.01	0.10	-0.04	0.05
18n.1n-13ny	-25.14	226.11	-0.755	0.13	0.04	-0.04	0.13	-0.03	0.05
18n.2o-18n.1n	-32.98	202.94	-0.566	0.87	0.32	-0.29	1.33	-0.39	0.71
19ny-18n.1n	-32.08	193.52	-0.588	0.71	0.25	-0.18	0.79	-0.17	0.28
20n.1n-18n.2o	-29.77	176.99	-0.623	0.58	0.18	-0.27	0.69	-0.37	0.47
20n.1o-20n.1n	-14.95	211.68	-0.931	1.75	0.63	-0.93	2.21	-1.29	1.52
21n.1n-20n.1o	0.35	205.51	-0.834	0.30	0.13	-0.16	0.45	-0.25	0.27
21n.1o-21n.1n	15.72	203.86	-0.929	0.86	0.30	-0.45	1.22	-0.64	0.75
22n.1n-21n.1n	2.01	219.66	-1.644	0.24	0.07	-0.10	0.40	-0.15	0.19
22n.1o-21n.1o	-5.49	221.70	-2.202	0.42	0.08	-0.17	0.64	-0.22	0.27
23n.1n-22n.1n	-8.87	194.03	-1.349	0.36	0.03	-0.09	0.45	-0.04	0.20
23n.2y-22n.1o	-9.27	198.44	-1.608	0.78	-0.02	-0.22	0.68	0.00	0.27
23n.2o-23n.1n	-7.26	203.69	-1.914	1.20	-0.04	-0.23	0.95	0.21	0.57
24n.1r-23n.1n	-8.38	216.90	-2.686	0.69	0.82	0.23	1.67	0.62	0.33
24n.3n-23n.2y	-8.63	199.95	-1.662	0.49	0.36	0.02	0.87	0.29	0.19
24n.3n-23n.2o	-9.80	205.82	-1.763	0.92	0.71	0.11	1.72	0.61	0.40
24n.3o-24n.1r	9.56	86.73	-1.507	3.65	4.88	3.22	9.23	6.16	5.56
25y-24n.3o	-1.50	101.43	-2.064	0.31	0.07	0.20	0.49	0.20	0.38

26y-25y	-12.16	200.04	-1.652	2.49	-0.28	0.21	1.90	0.52	0.57
26o-25o	-12.10	201.75	-1.827	4.97	0.23	-0.09	2.78	1.66	1.22

These angular velocities specify India relative to Eurasia plate motion from the old to the young limits of the listed time intervals. The angular rotation rates $\dot{\omega}$, which are positive anticlockwise, are normalized to the GTS20 magnetic reversal ages in Supplemental Table 1. The angular velocities and Cartesian covariances, which are tied to the India plate, are derived from the Table 4 finite rotations, whose covariances are also tied to the India plate. The covariances, which have units of 10^{-6} radians^2 Myr^{-2}, The footnotes to Table 2 in the main document give further information about the covariances.

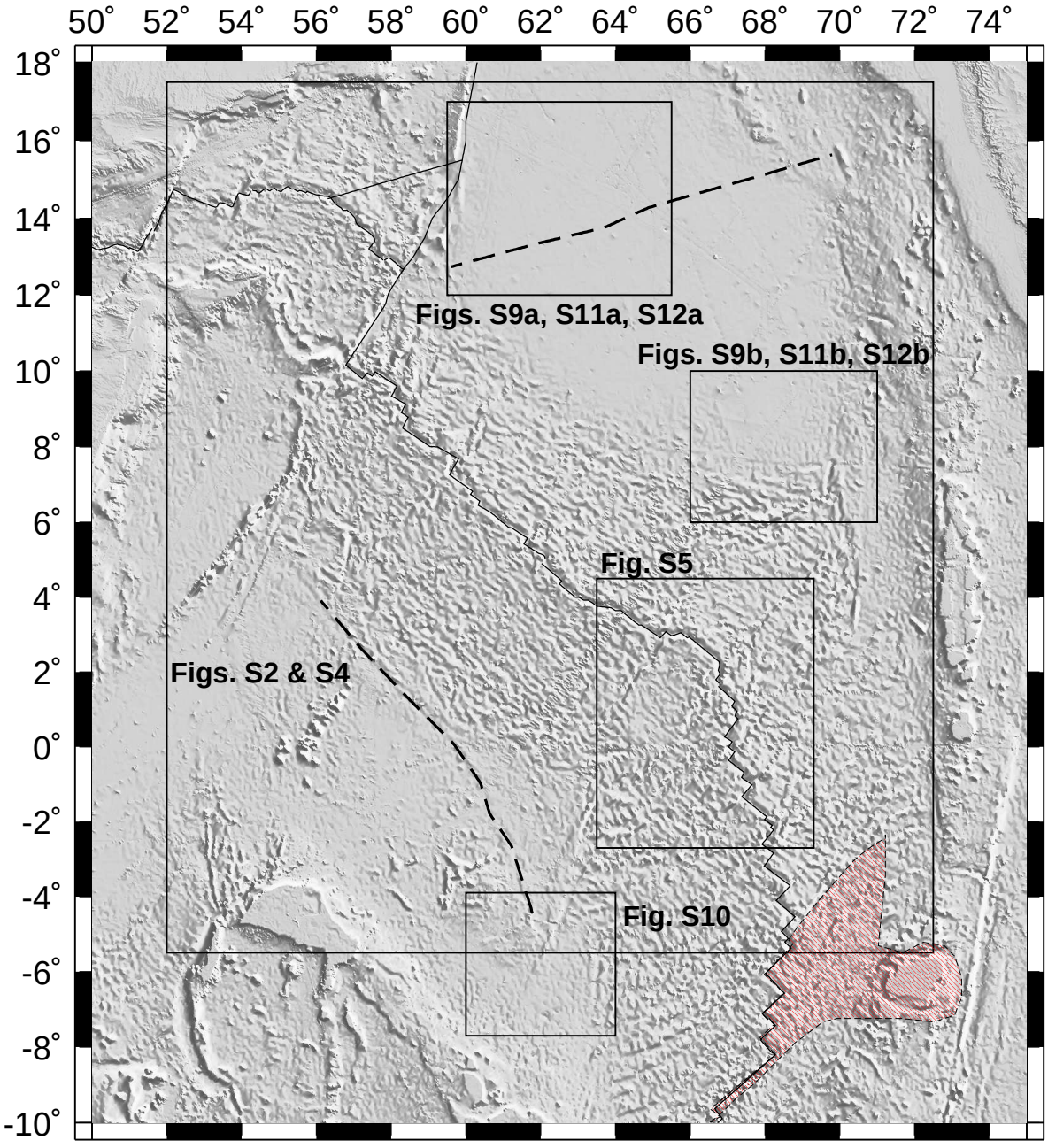

Figure S1. Location chart for supplemental figures that are maps.

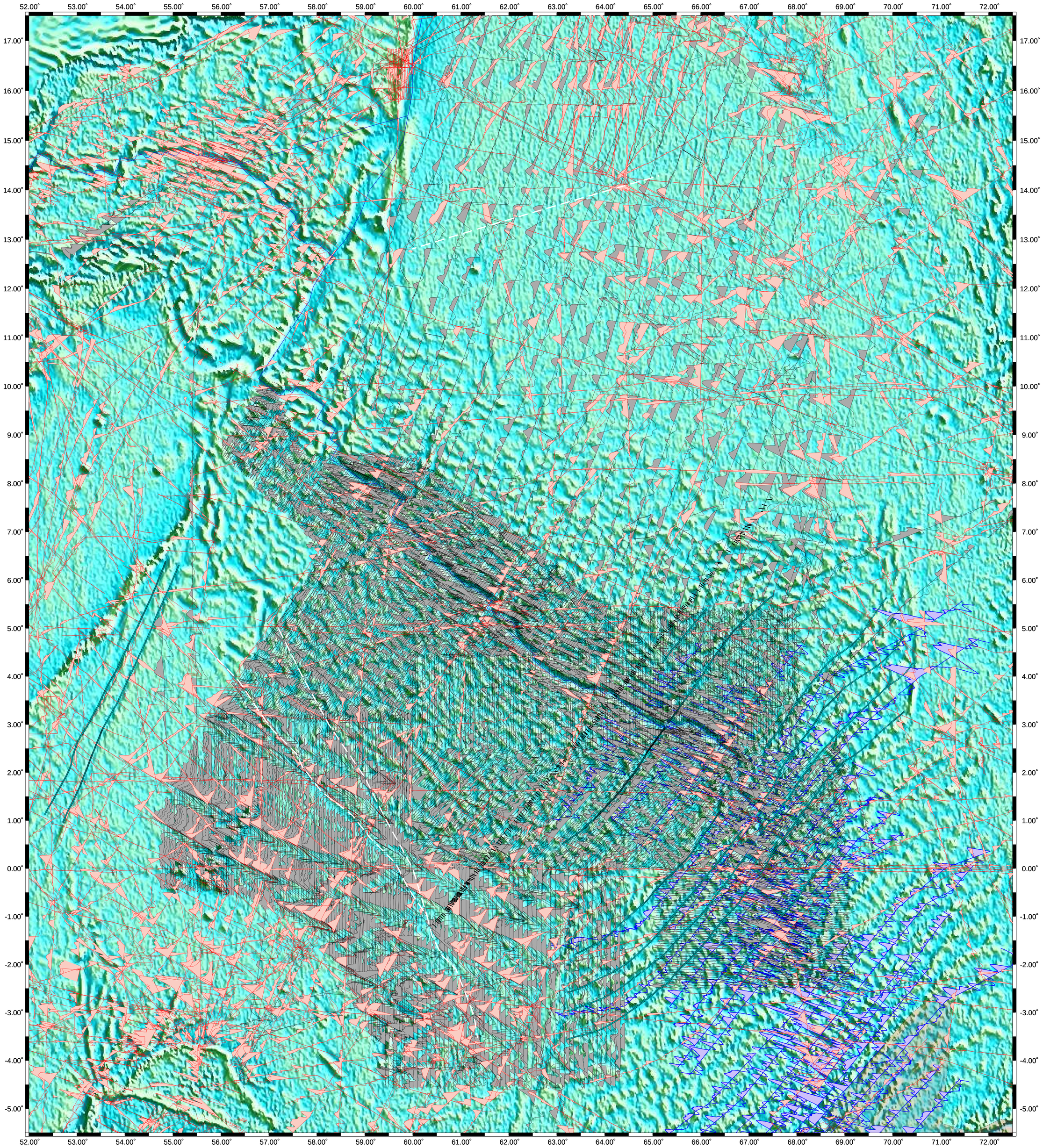

Figure S2. Along-track magnetic anomaly data used in the analysis overlaid on the vertical derivative of the 1-minute gravity field (version 29 available at ftp://topex.ucsd.edu/pub/global_grav_1min; Sandwell et al. 2014). Our interpretations and reconstructions of all 45 magnetic reversals and flow lines that are described in the main document are shown in Fig. S4. The sources of the data are indicated by the color and shading of each track, as follows: Red tracks and pink shading identify ship data available through the National Geophysical Data Center marine geophysical data archive. Blue tracks and shading identify Diego Garcia aeromagnetic data that are available through the same archive. The black tracks and gray shading show the Russian shipboard data that are described in the main document. Digitized fracture zone flow lines are shown by the aquamarine circles. The best-fitting reconstructed flow lines are shown in Fig. S4.

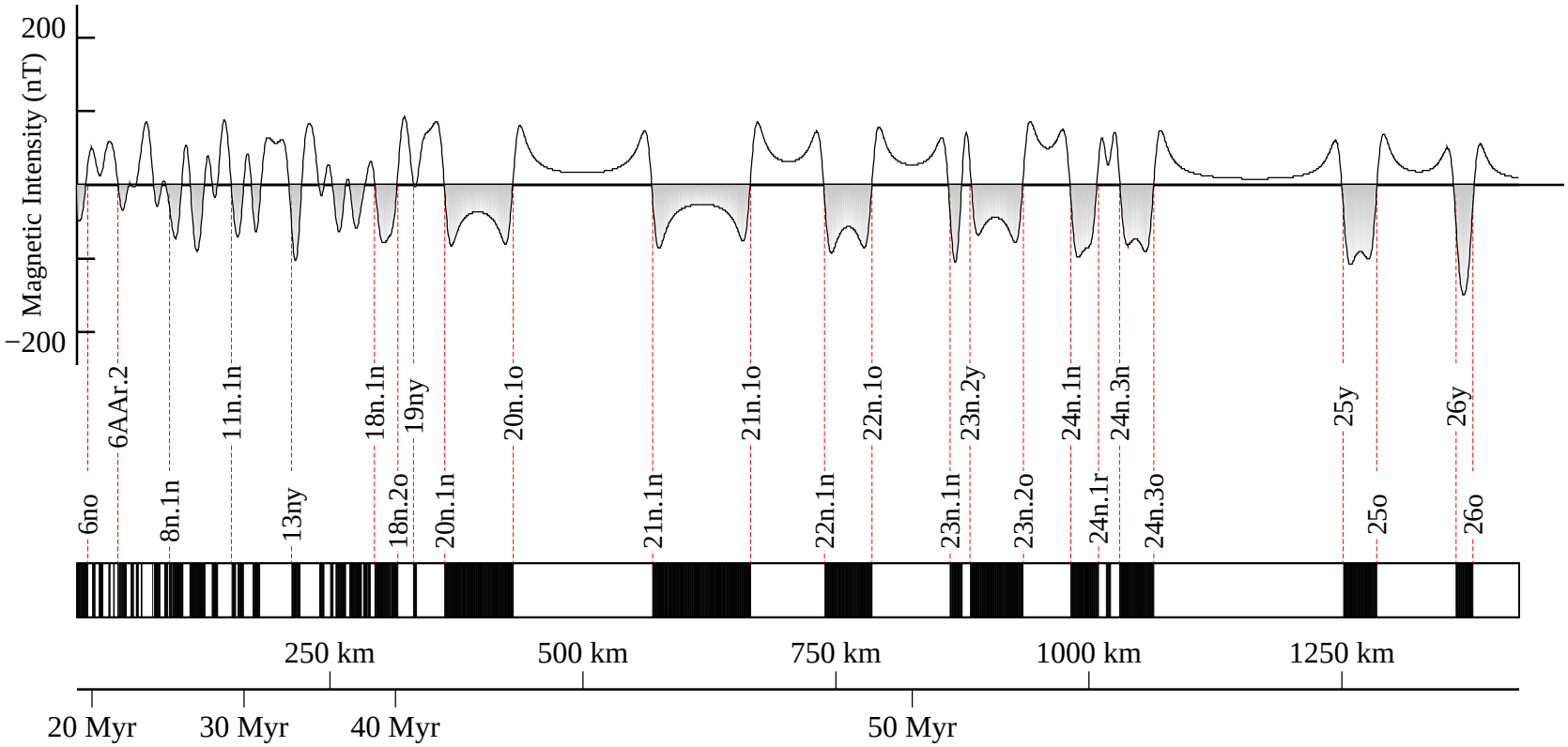

Supplemental Figure 3. Reversal correlation points between magnetic anomalies 26n and 6 and magnetic block model used for our study. The synthetic magnetic profile was calculated using a model with half−spreading rates of 15 mm yr^{-1} for 20−42 Ma and 60 mm yr^{-1} for times before 42 Ma, similar to that estimated for our study area. The synthetic profile further uses a ridge azimuth of N54ºW, a 3−km−wide reversal transition zone, and ambient and paleomagnetic inclinations and declinations for a point near the center of the Carlsberg Ridge (3.6ºN, 64.2ºE). The shaded anomalies occurred during periods of normal magnetic field polarity.

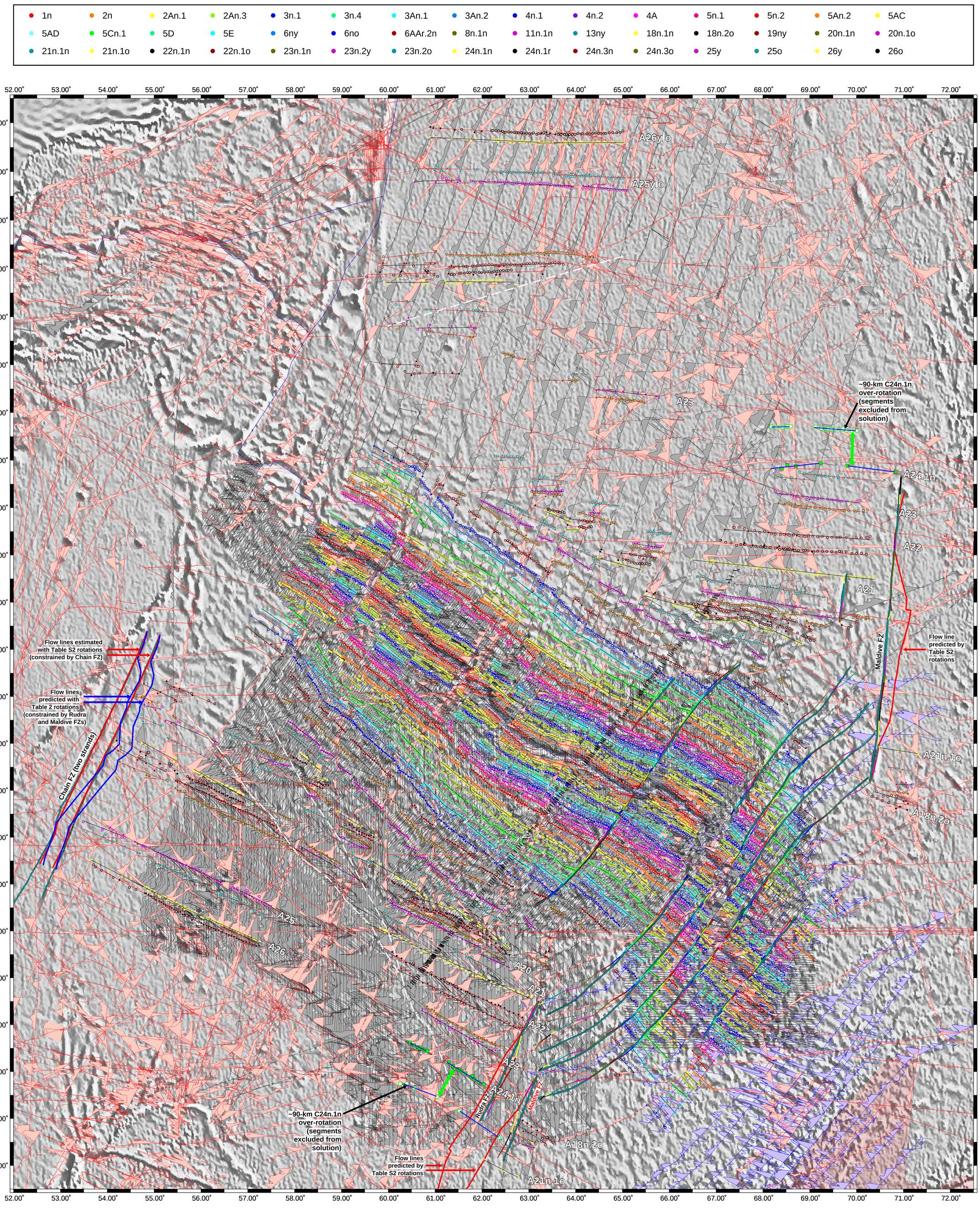

Figure S4. (NOTE TO VIEWER: This graphic is best viewed when magnified 200 percent or more). Along-track magnetic anomaly data from Fig. S2 with our interpretations and reconstructions of all 45 magnetic reversals and flow lines that are described in the main document. The colors that are used to identify each magnetic reversal are defined in the legend above the figure. The solid and open circles identify the reversal crossings at their original locations and their locations reconstructed with the Table 2 best-fitting rotations. The black and red lines show the great circles that best fit the stationary and rotated reversal crossings for each paleo-spreading segment. The original (digitized) fracture zone flow lines are shown by the aquamarine circles. The colored circles that are used to represent the fracture zone flow lines estimated with the Table 2 rotations use the same color coding found in the legend above the figure. The red flow lines are Chron 20n.1n to Chron 26o flow lines predicted by the rotations from Supplemental Table 1, which are constrained by the Chain fracture zone strands during C20-C26 time rather than the Maldive and Rudra fracture zones. The blue flow lines along the Chain FZ strands south of the westernmost Carlsberg Ridge are predicted with the Table 2 rotations, which optimize the fits to the Rudra and Maldive FZs at the eastern end of the Carlsberg Ridge. The poor fits of the Table 2 rotations to the Chain FZ and the Supplemental Table 2 rotations to the Rudra and Maldive FZs illustrate the inconsistency of the FZs at the two ends of the ridge for constraining India-Somalia rotations for times earlier than C21. See the Fig. S2 caption for other information.

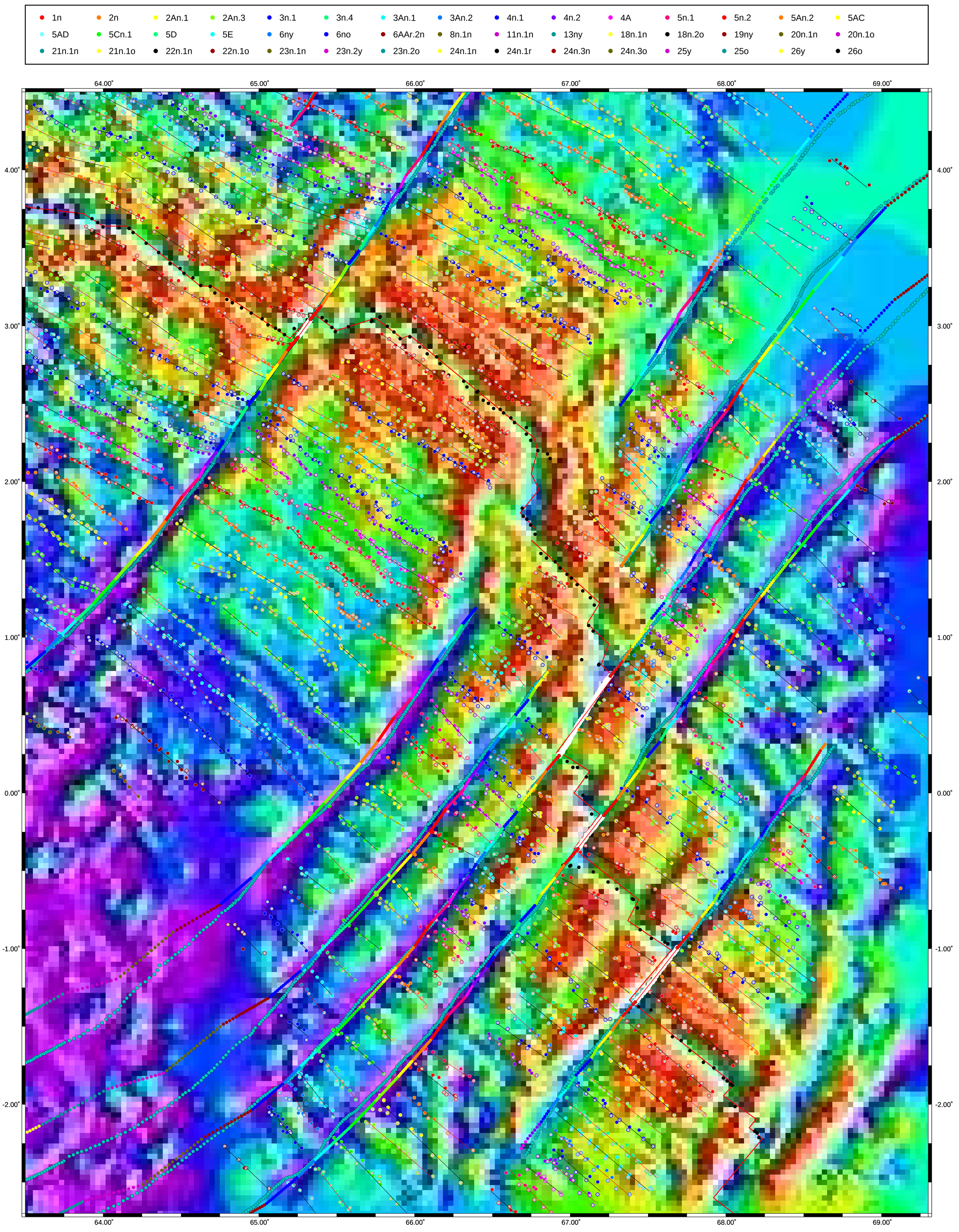

Figure S5. Reconstructions of all 45 magnetic reversals, fracture zone flow lines, and transform faults with Table 2 rotations overlaid on a 3-km-resolution bathymetric grid derived from depth measurements along the ship tracks displayed in Fig. 2 of the main document. The reconstructions in this figure focus on the subregion of Supplemental Figure 4 with the four transform faults that constrain the C1n rotation and the bathymetric constraints on the transform fault traces. The thick white lines near 3˚N, 65.25˚E, 0.5˚N, 0.3˚S, and 1.2˚S identify the digitized traces of the four transform faults; the red lines that overlay the digitized transform fault traces are the small circles around the best-fitting Chron 1n pole from Table 2. The large black circles along the ridge axis identify the center of Chron 1 and thus approximate the ridge axis. See the caption for Supplemental Figure 4 for other information.

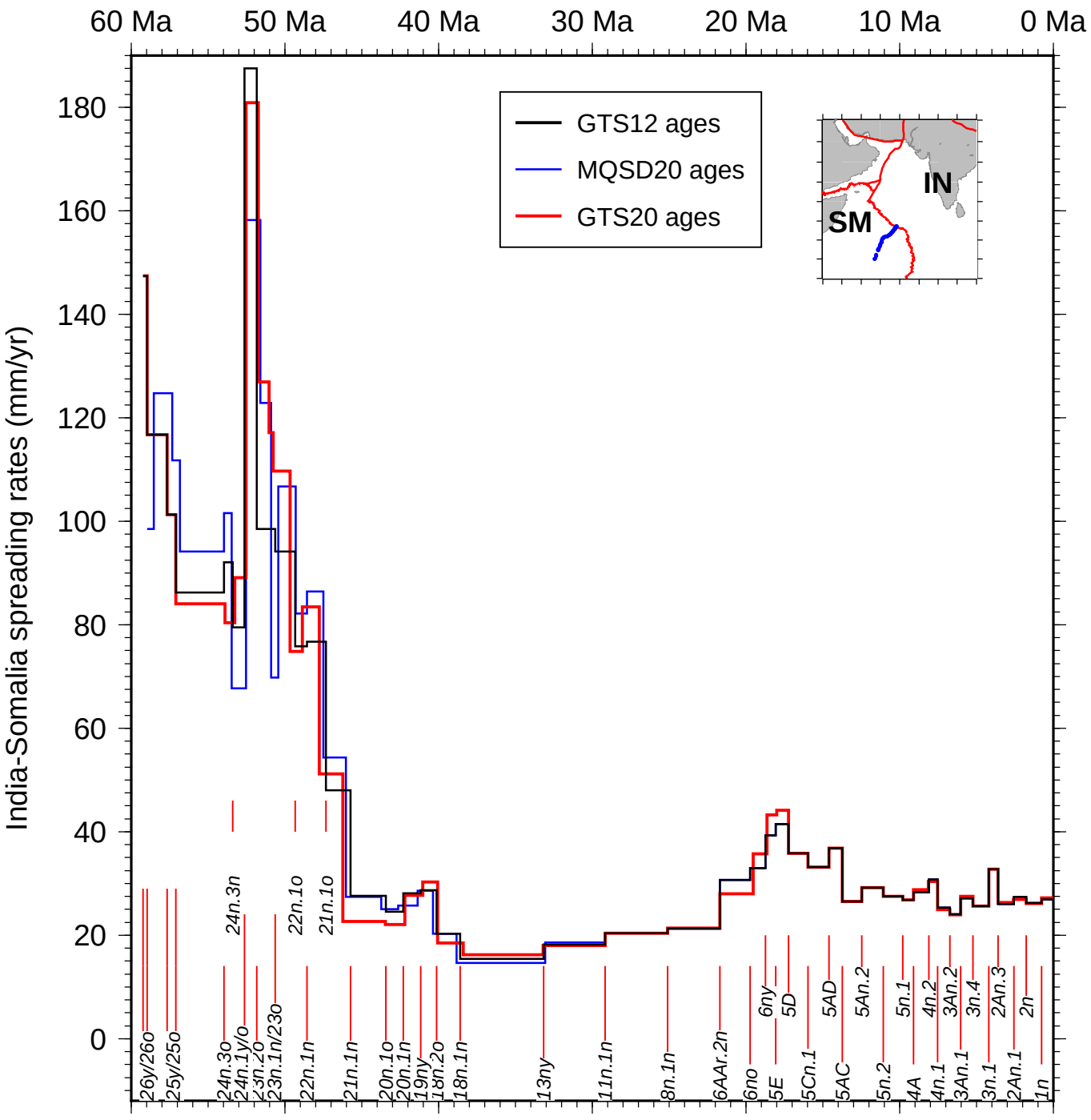

Supplemental Fig. 6. India relative to Somalia spreading rates estimated with angular velocities derived from the Table 2 best-fitting finite rotations and reversal ages from GTS12 (black line), GTS2020 (red line) and Malinverno et al. (2020) (MQSD20 label and blue line). The spreading rates are estimated along the Somalia plate flow line indicated in the inset map All rates are corrected for outward displacement. Abbreviations: IN, India; SM, Somalia.

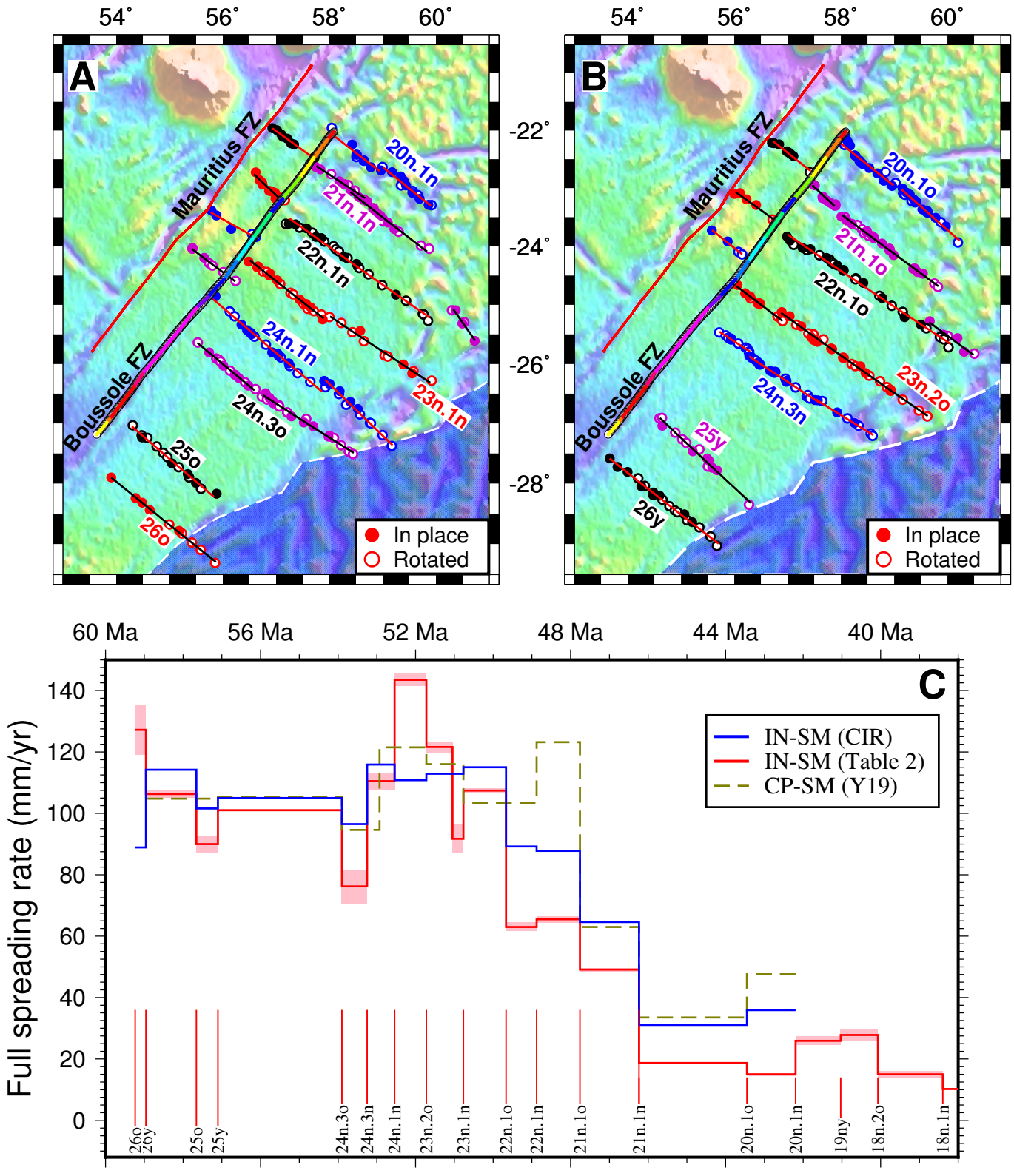

Supplemental Figure 7. A and B - Best fitting reconstructions of C26 to C20 reversal crossings from the Capricorn plate onto the Somalia plate corrected for Capricorn-India plate motion since 16 Ma (see text). The reversal crossings are from sources referenced in the text. The multicolored and red lines respectively show the fit of the best fitting rotations to the Boussole fracture zone, which was used to estimate the rotations, and the Mauritius fracture zone, which was not. C - Comparison of India-Somalia (IN-SM) spreading rates from Fig. 22a (red line) to Capricorn-Somalia (CP-SM) rates (normalized to GTS20) estimated with Yahteesh et al. (2019) rotations (dashed green line) and rates estimated with the rotations that best fit the data shown in Panels A and B (blue line) for a flow line through the data shown in Panels A and B.

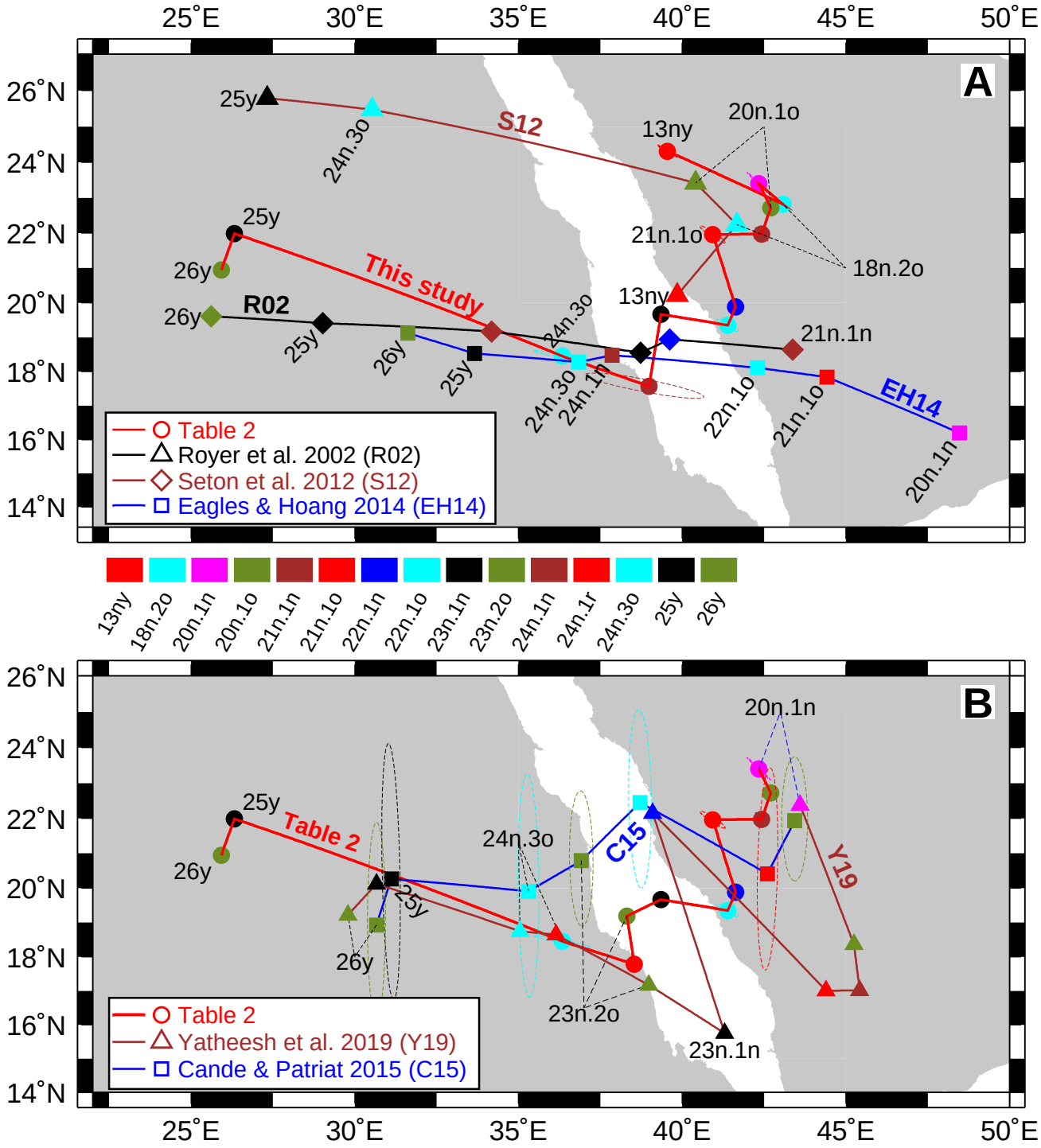

Supplemental Figure 8. (A) Comparison of finite opening poles from this study, Royer et al. (2002), Seton et al. (2012), and Eagles and Hoang (2014) for Chron 13 and older from reconstructing Carlsberg Ridge (India-Somalia) reversal and fracture zone crossings. The ellipses show the 2-D 95 percent confidence regions. (B) Comparison of Chron 20 and older finite opening poles from this study (Table 2) to Cande & Patriat (2015) and Yatheesh et al. (2019) opening poles that reconstruct southern Central Indian Ridge (Capricorn-Somalia) reversal and fracture zone crossings. In order to compare the latter poles to the India-Somalia poles in Table 2, the Capricorn-Somalia rotations have been corrected for the movement of the Capricorn plate relative to India since C5Cn.1 (16 Ma) as follows: $\Omega^{\text{Capricorn}\rightarrow\text{India}}\ \Omega^{\text{Somalia}\rightarrow\text{Capricorn}}$, where the latter rotation accounts for all Capricorn-India plate motion since the postulated initiation of movement between the two plates at the time of Chron 5Cn.1 (~16 Ma) (Bull et al. 2010). The poles that are shown from Table 2 are limited to poles that were estimated in the studies cited above. Selected poles are labeled to facilitate the comparison.

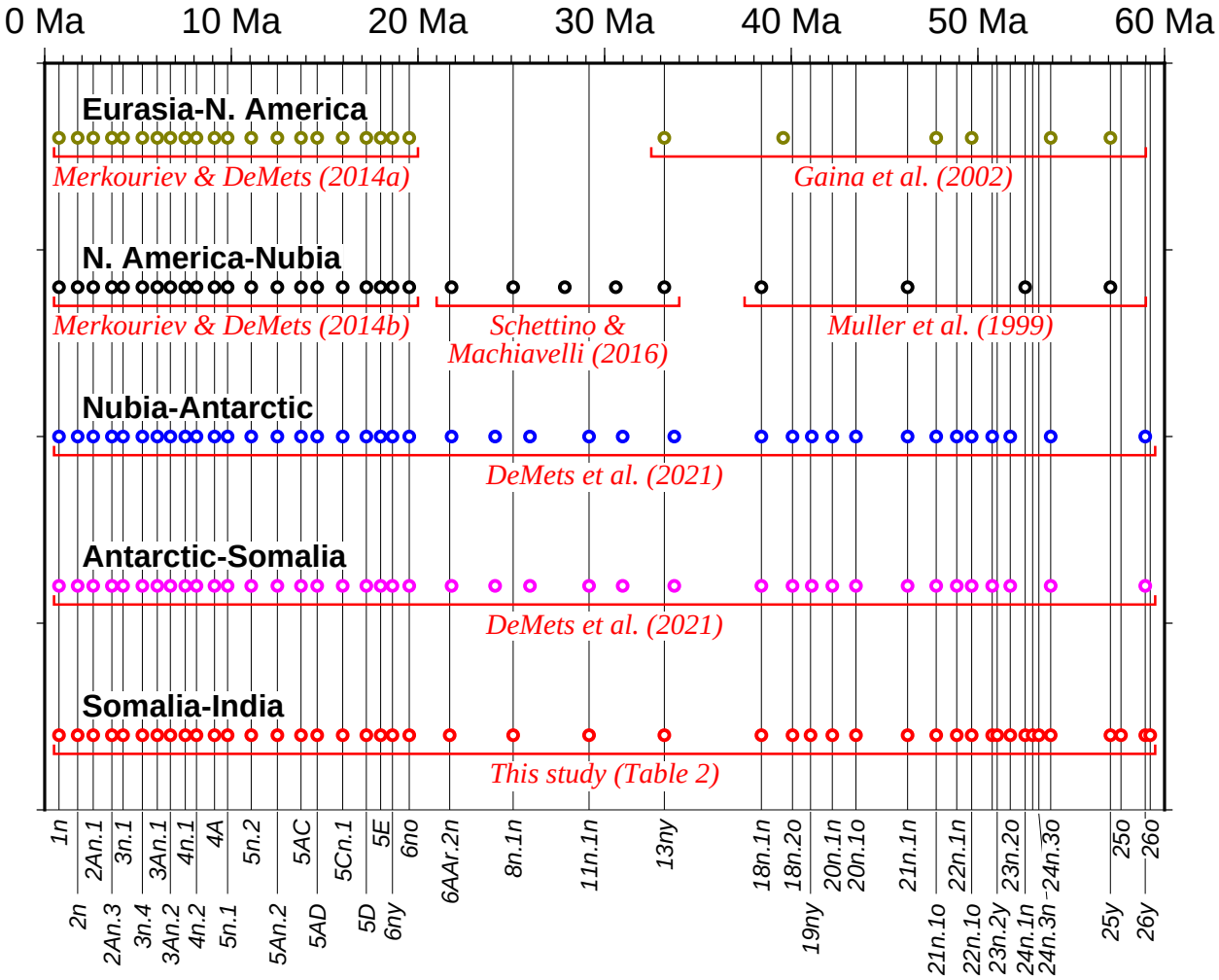

Supplemental Figure 9. Plate circuit rotations that constrain the India-Eurasia rotations in Table 4 of the main document. The circles indicate the times for which rotations have been estimated by ourselves or other authors from magnetic reversal and fracture zone reconstructions at the times indicated at the bottom of the figure. The vertical lines indicate the interpolation ages that we used for our India-Eurasia rotations; each interpolation age corresponds to one of the 45 reversals that were reconstructed in this study for the India-Somalia plate pair (Table 2). All interpolated rotations were estimated from rotations for the next oldest and youngest times. After interpolating the available finite rotations for each plate pair, we combined the interpolated rotation sequences as described in the main document in order to determine India-Eurasia rotations at all 45 times. The sources for the plate pair rotations are specified on the figure.

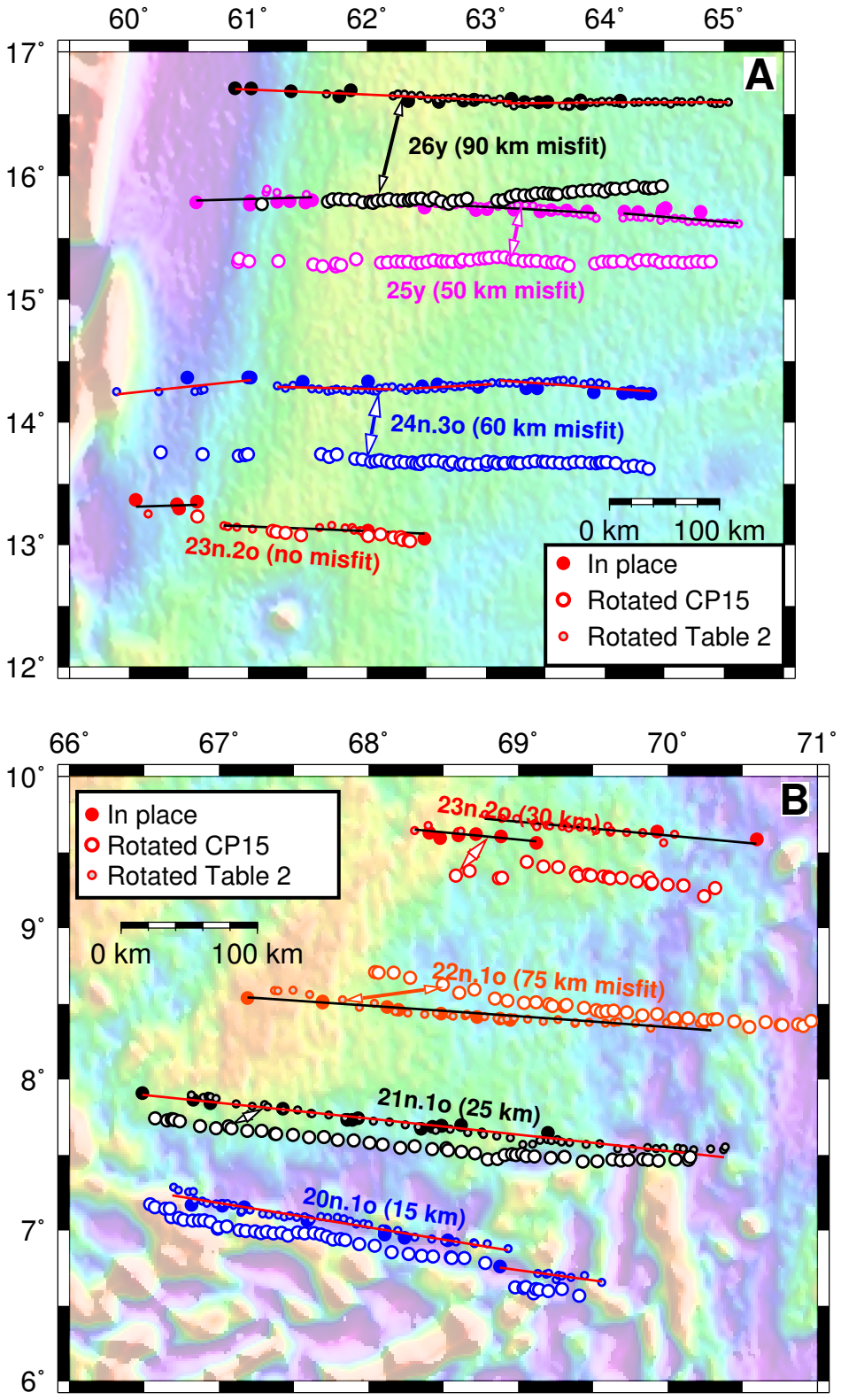

Supplemental Figure 10. Fits of Cande & Patriat (2015) (CP15) Capricorn-Somalia rotations to magnetic lineations C23n.2o to C26no along the western Carlsberg Ridge (Panel A) and magnetic lineations C20n.1o to C23n.2o along the eastern Carlsberg Ridge (Panel B) after correcting their $\Omega^{\text{Somalia}\rightarrow\text{Capricorn}}$ rotations as follows: $\Omega^{\text{Capricorn}\rightarrow\text{India}}\,\Omega^{\text{Somalia}\rightarrow\text{Capricorn}}$, where the latter rotation accounts for all Capricorn-India plate motion since the postulated initiation of movement between the two plates at the time of Chron 5Cn.1 (~16 Ma) (Bull et al. 2010). The double-headed arrows identify the misfits of the Cande & Patriat rotations. The Somalia plate reversal crossings in both panels are rotated onto the India plate. The red and black lines are the great circle segments that best fit the reversal crossings reconstructed with our best-fitting rotations.

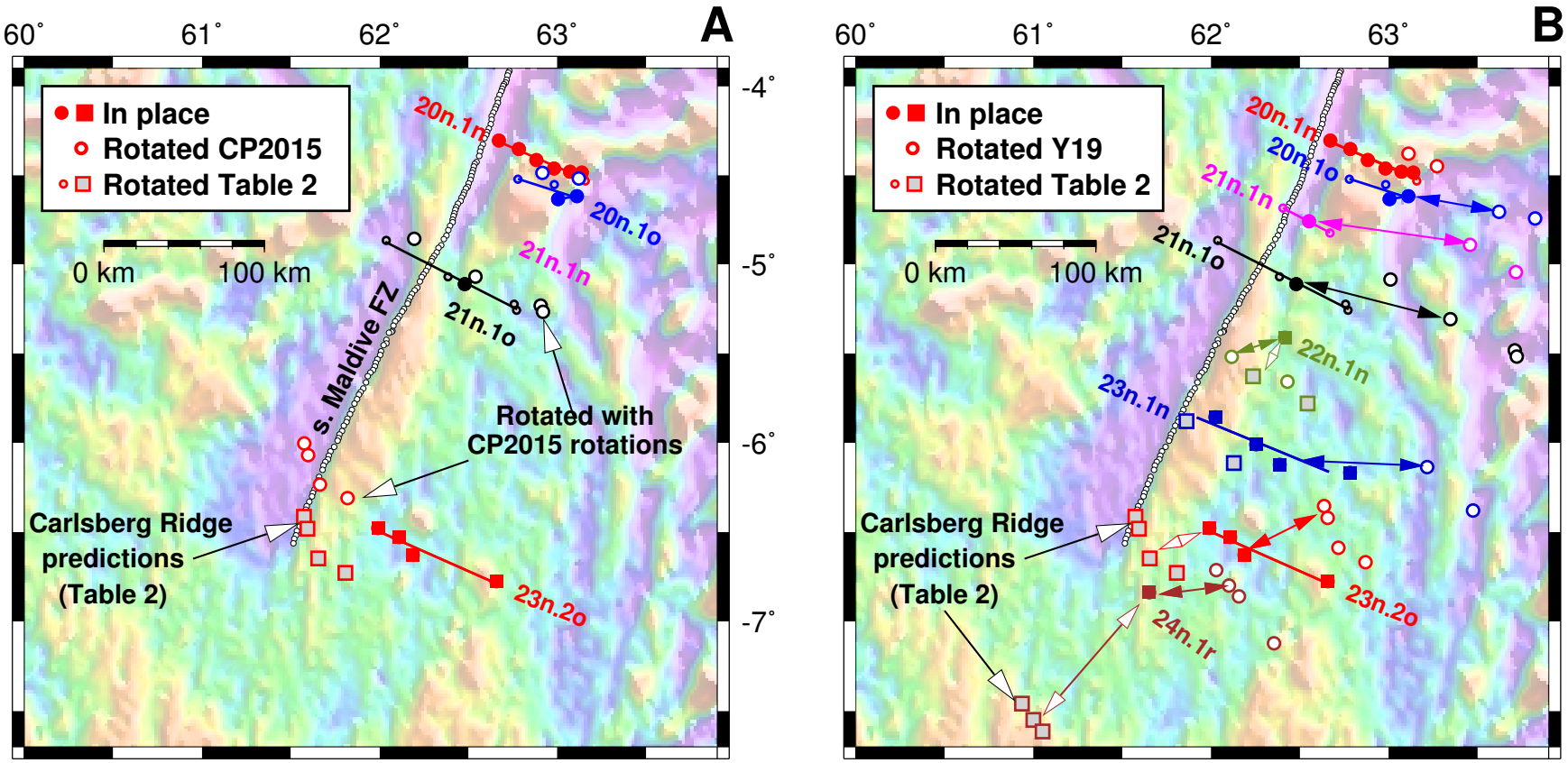

Supplemental Figure 11. (A) Comparisons of Table 2 rotation fits to Cande & Patriat (2015) Somalia-Capricorn rotation fits for C20n.1o to C23n.2o after correcting their $\Omega^{\text{Capricorn}\rightarrow\text{Somalia}}$ rotations as follows: $\Omega^{\text{Capricorn}\rightarrow\text{Somalia}}$ $\Omega^{\text{India}\rightarrow\text{Capricorn}}$. The latter rotation accounts for all Capricorn-India plate motion since the postulated initiation of movement between the two plates at the time of Chron 5Cn.1 (~16 Ma) (Bull et al. 2010). The Cande & Patriat rotations were estimated from Capricorn-Africa-Antarctic data. Fig. 16 from the main document shows the location of this area. (B) Same as Panel A but with the $\Omega^{\text{Somalia}\rightarrow\text{Capricorn}}$ rotations from Yakteesh et al. (2019). In both panels, India plate reversal crossings are rotated onto the Somalia plate. The colored lines are the great circle segments that best fit the reversal crossings reconstructed with our best-fitting Table 2 rotations. The reversals that are displayed in each panel are limited to the subset of reversals that were reconstructed by Cande & Patriat (2015) and Yakteesh et al. (2019). Abbreviations: CIR, Central Indian Ridge; CP2015, Cande & Patriat (2015); Y19, Yakteesh et al. (2019).

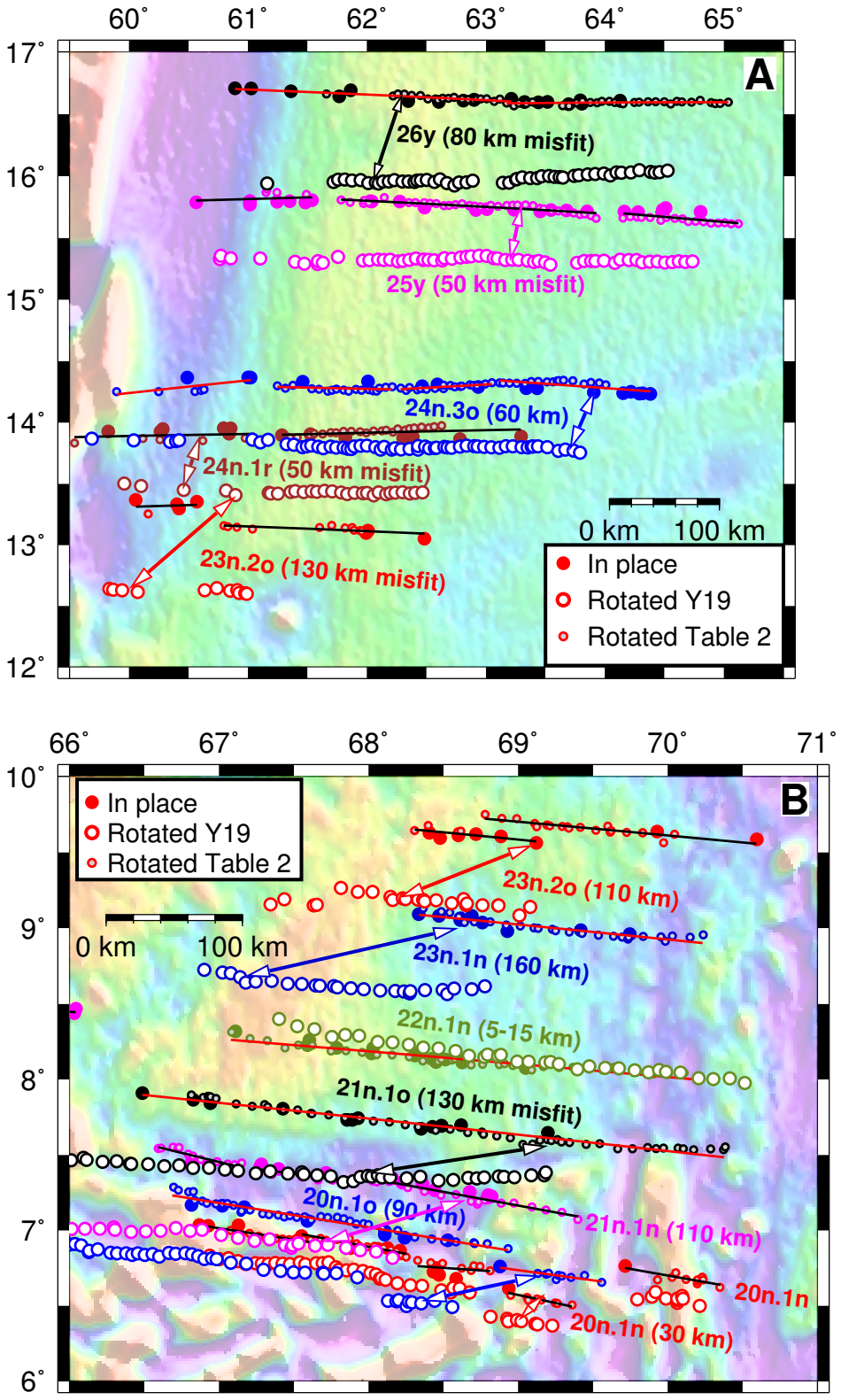

Supplemental Figure 12. Fits of Yatheesh et al. (2019) (Y19) Capricorn-Somalia rotations to magnetic lineations C23n.2o to C26no along the western Carlsberg Ridge (Panel A) and magnetic lineations C20n.1o to C23n.2o along the eastern Carlsberg Ridge (Panel B) after correcting their $\Omega^{\text{Somalia}\rightarrow\text{Capricorn}}$ rotations as follows: $\Omega^{\text{Capricorn}\rightarrow\text{India}}\,\Omega^{\text{Somalia}\rightarrow\text{Capricorn}}$, where the latter rotation accounts for all Capricorn-India plate motion since the postulated initiation of movement between the two plates at the time of Chron 5Cn.1 (~16 Ma) (Bull et al. 2010). The red and black lines are the great circle segments that best fit the reversal crossings reconstructed with our best-fitting Table 2 rotations. The double-headed arrows identify the misfits of the Yatheesh et al. rotations. The Somalia plate reversal crossings in both panels are rotated onto the India plate.

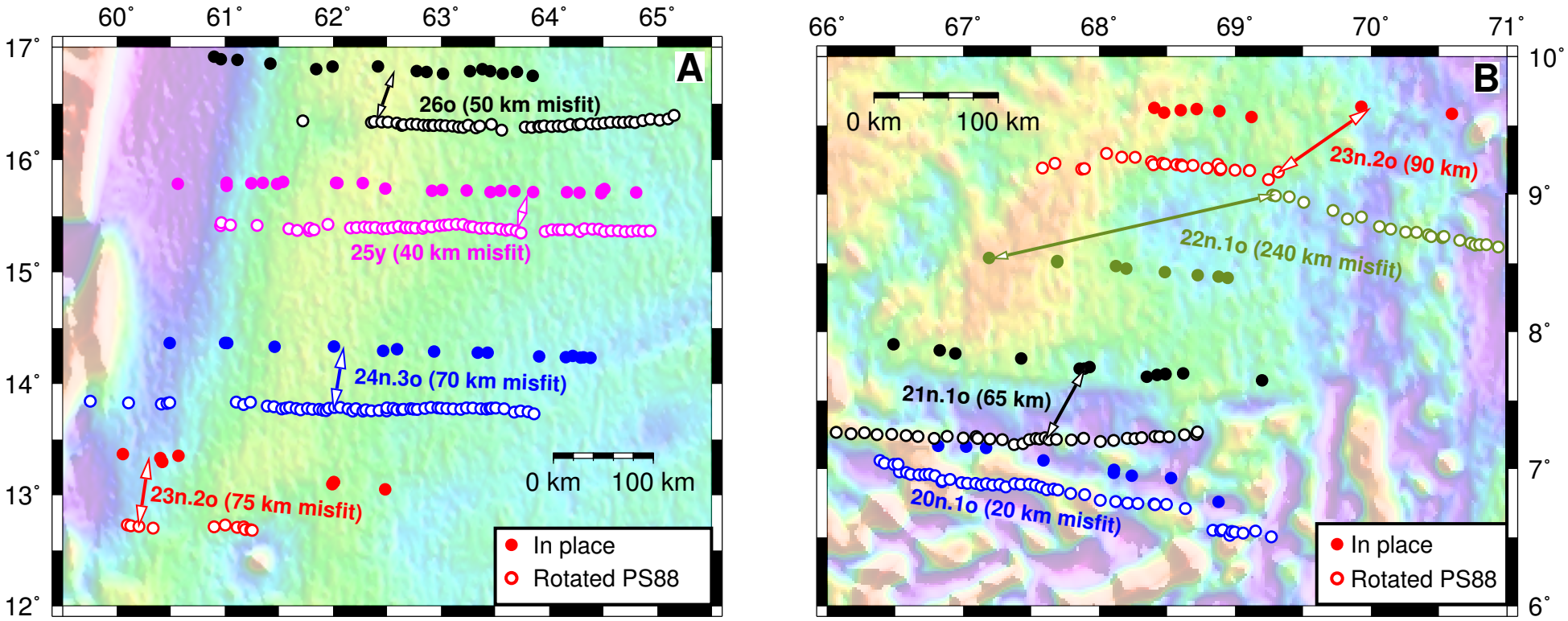

Supplemental Figure 13. Fits of Patriat & Segoufin (1988) (PS88) Capricorn-Somalia rotations to magnetic lineations C23n.2o to C26no along the western Carlsberg Ridge (Panel A) and magnetic lineations C20n.1o to C23n.2o along the eastern Carlsberg Ridge (Panel B) after correcting their $\Omega^{\text{Somalia}\rightarrow\text{Capricorn}}$ rotations as follows: $\Omega^{\text{Capricorn}\rightarrow\text{India}}$ $\Omega^{\text{Somalia}\rightarrow\text{Capricorn}}$, where the latter rotation accounts for all Capricorn-India plate motion since the postulated initiation of movement between the two plates at the time of Chron 5Cn.1 (~16 Ma) (Bull et al. 2010). The double-headed arrows identify the misfits of the rotations from PS88. The Somalia plate reversal crossings in both panels are rotated onto the India plate.